HELSINKI INSTITUTE OF PHYSICS INTERNAL REPORT SERIES

HIP - 2011 - 01

Position-sensitive silicon strip detector characterization using particle beams

Teppo Mäenpää

Helsinki Institute of Physics,
P.O.Box 64, FIN-00014 University of Helsinki, Finland

ACADEMIC DISSERTATION

To be presented, with the permission of the Faculty of Science of the University of Helsinki, for public criticism in the Auditorium 1 (Psychology A132) at Siltavuorenpenger 1 A, Helsinki, on Friday May 20th 2011, at 12 o'clock.

Helsinki 2011

ISBN 978–952–10–5325–2 (paperback)
ISBN 978–952–10–5326–9 (pdf)
ISSN 1455 – 0563
http://ethesis.helsinki.fi
Helsinki University Press 2011

Abstract

Silicon strip detectors are fast, cost-effective and have an excellent spatial resolution. They are widely used in many high-energy physics experiments. Modern high energy physics experiments impose harsh operation conditions on the detectors, e.g., of LHC experiments. The high radiation doses cause the detectors to eventually fail as a result of excessive radiation damage. This has led to a need to study radiation tolerance using various techniques. At the same time, a need to operate sensors approaching the end their lifetimes has arisen.

The goal of this work is to demonstrate that novel detectors can survive the environment that is foreseen for future high-energy physics experiments. To reach this goal, measurement apparatuses are built. The devices are then used to measure the properties of irradiated detectors. The measurement data are analyzed, and conclusions are drawn.

Three measurement apparatuses built as a part of this work are described: two telescopes measuring the tracks of the beam of a particle accelerator and one telescope measuring the tracks of cosmic particles. The telescopes comprise layers of reference detectors providing the reference track, slots for the devices under test, the supporting mechanics, electronics, software, and the trigger system. All three devices work. The differences between these devices are discussed.

The reconstruction of the reference tracks and analysis of the device under test are presented. Traditionally, silicon detectors have produced a very clear response to the particles being measured. In the case of detectors nearing the end of their lifefimes, this is no longer true. A new method benefitting from the reference tracks to form clusters is presented. The method provides less biased results compared to the traditional analysis, especially when studying the response of heavily irradiated detectors. Means to avoid false results in demonstrating the particle-finding capabilities of a detector are also discussed.

The devices and analysis methods are primarily used to study strip detectors made of Magnetic Czochralski silicon. The detectors studied were irradiated to various fluences prior to measurement. The results show that Magnetic Czochralski silicon has a good radiation tolerance and is suitable for future high-energy physics experiments.

List of Publications

This thesis consists of an overview and the following publications:

I C. Eklund, A. Heikkinen, A. Honkanen, V. Karimäki, **T. Mäenpää**, E. Pietarinen, H. Saarikoski, K. Skog, J. Tuominiemi, T. Tuuva *Silicon beam telescope for CMS detector tests*, Nuclear Instruments and Methods in Physics Research Section A: Accelerators, Spectrometers, Detectors and Associated Equipment 430 (1999) 321–332

II **T. Mäenpää**, E. Hæggström, E. Anttila, A. Onnela, T. Lampén, P. Luukka, V. Karimäki, J. Tuominiemi *Finnish CMS-TOB cosmic rack*, Nucl. Instr. and Meth. A 570 (2007) 258–261

III **T. Mäenpää**, P. Luukka, B. Betchart, S. Czellar, R. Demina, Y. Gotra, M. Frey, F. Hartmann, J. Härkönen, S. Korjenevski, M.J. Kortelainen, T. Lampén, B. Ledermann, V. Lemaitre, T. Liamsuwan, O. Militaru, H. Moilanen, H.J. Simonis, L. Spiegel, E. Tuominen, E. Tuovinen, J. Tuominiemi, *Silicon beam telescope for LHC upgrade tests*, Nucl. Instr. and Meth. A 593 (2008) 523–529

IV M.J. Kortelainen, T Lampén, H. Moilanen, **T. Mäenpää**, *Off-line Calibration and Data Analysis for the Silicon Beam Telescope on the CERN H2 Beam*, Nucl. Instr. and Meth. A 602 (2009) 600–606

V **T. Mäenpää**, H. Moilanen, D. Ungaro *FinnCRack, a cosmic muon telescope for detector studies*, Nucl. Instr. and Meth. A 604 (2009) 269–272

VI P. Luukka, J. Härkönen, **T. Mäenpää**, B. Betchart, S. Bhattacharya, S. Czellar, R. Demina, A. Dierlamm, Y. Gotra, M. Frey, F. Hartmann, V. Karimäki, T. Keutgen, S. Korjenevski, M.J. Kortelainen, T. Lampén, V. Lemaitre, M. Maksimow, O. Militaru, H. Moilanen, M. Neuland, H.J. Simonis, L. Spiegel, E. Tuominen, J. Tuominiemi, E. Tuovinen, H. Viljanen *Test beam results of heavily irradiated magnetic Czochralski silicon (MCz-Si) strip detectors*, Nucl. Instr. and Meth. A 612 (2010) 497–500

VII **T. Mäenpää**, M.J. Kortelainen, T Lampén *Track-induced clustering in position sensitive detector characterization*, IEEE Transactions on Nuclear Science, 57 4 (2010) 2196 – 2199

VIII Leonard Spiegel, Tobias Barvich, Burt Betchart, Saptaparna Bhattacharya, Sandor Czellar, Regina Demina, Alexander Dierlamm, Martin Frey, Yuri Gotra, Jaakko Härkönen, Frank Hartmann, Ivan Kassamakov, Sergey Korjenevski, Matti J. Kortelainen, Tapio Lampén, Panja Luukka, **Teppo Mäenpää**, Henri Moilanen, Meenakshi Narain, Maike Neuland, Douglas Orbaker, Hans-Jürgen Simonis, Pia Steck, Eija Tuominen, Esa Tuovinen *Czochralski Silicon as a Detector Material for S-LHC Tracker Volumes*, Nucl. Instr. and Meth. A 628 (2011) 242 – 245

Author's contribution

I This article was the authors first hands-on experiment. The device was designed and the paper mostly written by more senior members of the research team. The author had a significant role in commissioning and operating the system described in the paper.

II All the work leading to this article except the mechanics was done by the author or undergraduate students under the author's direct supervision.

III In the work leading to this article, the author was responsible for the data acquisition system and contributed to the off-line analysis.

IV This is a co-authored description of the SiBT07 analysis code. The SiBT07 analysis code itself was implemented mostly by others, on the basis of experience of the FinnCRack analysis code which was implemented by the author on top of an older version of the analysis framework.

V The author coordinated the data acquisition and both designed and implemented the data analysis. The safety system described in the article was built by others.

VI The author was in charge of the data acquisition, analyzed the data and participated in interpreting the results.

VII The author orchestrated everything and actively participated in all the fields of work needed to make this paper.

VIII The author was in charge of the data acquisition, co-analyzed the data and participated in interpreting the results.

Contents

Chapter 1

Background

This work was done in the framework of the Compact Muon Solenoid (CMS) upgrade project. The following sections give a short description of the LHC collider, CMS experiment, and CMS upgrade as background information to the study.

1.1 The Large Hadron Collider

An event where two elementary particles collide, studied by observing the particles that are produced in the collision, provides insights into matter being studied in modern high-energy physics.

The Large Hadron Collider (LHC), located on the Laboratory of Particle Physics of the European Organization for Nuclear Physics (CERN) at the Swiss-French border, is the newest collider that produces these primary events. The LHC is a circular particle collider with the circumference of 27 kilometers, situated approx. 100 meters underground [1]. The protons arrive in the LHC with the energy of 450 GeV from the Super Proton Synchrotron (SPS), which in turn is preceded by the Proton Synchrotron (PS), the Booster, and Linear Accelerator (LINAC) which provides the protons to the CERN accelerator system. Once the LHC reaches its design capacity, it provides proton-proton collisions with up to 14 TeV of energy.

Circular accelerators use different kinds of magnets, to keep the particles in their desired circular path. The LHC accelerates particles in groups called bunches. Every particle in a bunch must be of the same type and have the same electric charge and therefore they repel each other. Focusing magnets in the collider keep the particle in the bunches in their desired orbits. Two accelerated particle bunches, moving in opposite directions, intersect at pre-determined collision points. A bunch crossing occurs once every 25 ns. There are 2×2808 bunches of 10^{11} particles circulating at relativistic speeds, and around 20 proton-proton collisions happen in a typical bunch crossing. One single bunch can be collided hundreds of millions of times before the LHC must be re-filled.

The protons are composite particles. The vast majority of the signals seen in the detectors of the LHC experiments are caused by protons breaking apart in an uninteresting way — only a small fraction of the signals that are seen represent particles produced at the hard collision of two elementary constituents of a proton. The LHC is able to collide lead ions in addition to protons, and one of the experiments, ALICE [2], was designed to study the physics questions of such interactions.

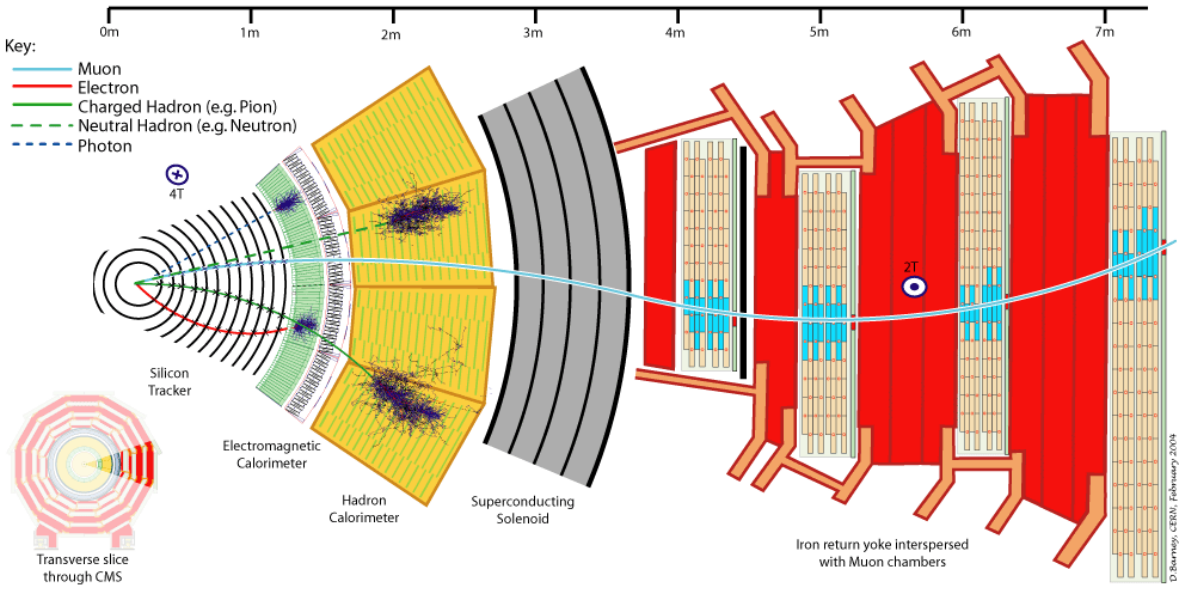

Figure 1.1: Illustration showing the subdetectors of the CMS experiment [3].

1.2 The Compact Muon Solenoid

The Compact Muon Solenoid (CMS) is one of the four large experiments at the LHC collider, located at one of the eight collision points. The main components of the CMS are depicted in Fig. 1.1. A large fraction of the recent Finnish contribution to CERN has taken place within the CMS collaboration, and hence this section concentrates on the CMS experiment.

The interesting phenomena studied by LHC experiments are too short-lived to be detected directly. Each decays into other particles at so-called primary vertex, which might decay further into something else at so-called secondary vertices. High Energy Physics (HEP) experiments measure the properties of these decay products and reconstruct the event in order to study the properties of the primary particles. The particles that eventually make it to the actual detectors of the LHC experiments are stable, or at least relatively long-lived, such as the muon ($t_{1/2} = 2.2\mu s$).

To be able to reconstruct the event, the experiments need to measure the momentum, energy, point of origin and identity of the decay products. The momentum of a charged particle in a magnetic field can be extracted from the curvature of its track, if the track is measured precisely enough. The tracks can also be used to measure the position of secondary vertices. Reliable identification of secondary vertices even when they reside close to the interaction point, is important for the identification of short-lived particles, such as B particles and τ leptons. This requires high-precision positional information of the helix-shaped track when it has been extrapolated from the tracker volume into the vicinity of the interaction point.

To match the speed and precision requirements at the LHC, the tracking detector of the Compact Muon Solenoid experiment [4] (CMS) is made of fast silicon sensors. These detectors measure the position of the particle when the particle passes through the detector. To reconstruct a track, several measurement points of each track and hence several detectors layers are needed: Ten layers of strip detectors surrounding three layers of pixel detectors. There are a total of 15 200 strip detector modules in silicon layers with a total of 10 million channels, together with another 65 million channels in the innermost pixel layers, to keep channel occupancy low.

This tracker is surrounded by an electromagnetic calorimeter, a hadronic calorimeter, and muon chambers. The calorimeters measure the total energy of the particles by stopping the par-

ticles and measuring the amount of energy deposited to the calorimeter by those particles. The tracker distracts the operation of the calorimeters since the initial energy of the particle is of interest, not the one they have after a passage through the tracker. There is a trade-off between the size[1] of a tracker and the quality of the calorimeter results.

A hadron collider event is an ill-posed inverse problem: different initial particles can have a similar mixture of end products. Usually only a small fraction of the interactions, such as 1/10 000 000 000 000, are interesting for a phenomenon being studied and a large number of such interactions is needed to obtain the desired results.

A trigger system in the context of a HEP experiment is used to select the interesting interactions that require detailed analysis. In the case of the CMS, only a fraction of the detector data is initially processed. The first-level trigger causes all the detector data of the triggered events to be read out and passed forward. Only events accepted by the high-level trigger are stored.

1.3 Future experiments

The radiation levels inside the LHC experiments are high, particle flux being above $10^6\,cm^{-2}\mathrm{s}^{-1}$ for the tracker when the LHC is running at its design luminosity. Over time, the accumulating radiation damage degrades the performance of the components of the CMS. The CMS components have been designed to survive throughout the originally-planned lifetime of the LHC.

In the proposed LHC upgrade [5], the luminosity of the collider will increase further. This is a relatively affordable way to allow a large number of new discoveries [6] to be made in the field of high-energy physics without the need to build a new collider and the associated experiments.

In this Super-LHC (SLHC) era, the detectors of today's tracker will no longer be a feasible option as a result of the further increase in radiation levels [7]. The current strip detectors were designed to withstand the fluence of $1.6 \times 10^{14}\,\mathrm{n}_{eq}/\mathrm{c}m^2$ [8] for the innermost part, while the fluences foreseen for the CMS tracker at the end of the SLHC running vary from $2 \times 10^{15}\,\mathrm{n}_{eq}/\mathrm{c}m^2$ for the innermost strip layer to $1.2 \times 10^{14}\,\mathrm{n}_{eq}/\mathrm{c}m^2$ for the outermost part [5]. The corresponding fluence for the innermost part of the pixel tracker would be $1.5 \times 10^{16}\,\mathrm{n}_{eq}/\mathrm{c}m^2$. Therefore, research studying radiation-tolerant silicon detectors that could be used as detector material in the trackers of the future experiments are needed. Characterizing prototype detectors and demonstrating that they can be used to find particles after being exposed to high radiation doses are two important steps in that research.

The radiation tolerance of the front-end electronics is also an issue [9, 10]. The increasing occupancy of the silicon strip detectors needs to be taken into account: the channel occupancy of the present detectors would be too high in the fluencies that are foreseen. Consequently, the tracker would need to be re-designed even if the radiation tolerance of the present detectors was not a factor.

[1] The particle loses energy when it interacts with the material that make up the tracker. The amount and type of material is important, not the tracker volume itself. The actual sensors of the tracker form only a small fraction of the total tracker mass.

Chapter 2

Introduction

The work presented in this thesis has its roots in High Energy Physics (HEP) experiments. A large fraction of the work leading to this thesis was motivated by a radiation tolerance study of strip detectors made of the Czochralski silicon material [11, 12, 13, 14, 15, 16]. This chapter provides a brief introduction to beam testing and the detectors being tested. while the following chapters limit the scope of discussion to the characterization of silicon strip detectors using highly energetic particles and a reference measurement.

2.1 Detectors

A particle can be detected, if it interacts with the active detector material. The detectors studied here are solid state detectors that produce the primary signal via the ionization of material[1]. Historically, gaseous detectors have dominated in the field of position-sensitive detectors. The gaseous detectors can cover large volumes in a more affordable construction. On the other hand, the active volume of solid state detectors is more dense and therefore provides more ionization in unit volume. Gaseous detectors can respond to this challenge by easier production of proportional counters. In other words, ionized particles can easily accelerate to high enough energies to provide secondary ionization [17]. Usually, only electrons (not the gaseous ions) are allowed to multiply, to keep the response linear. In solid state detectors, signal amplification in the detector material would require very high electric fields and is usually not done. Solid state detectors are usually fast compared to gaseous detectors, which can be important in high-luminosity colliders. From now on, only solid state semiconductor detectors are discussed.

The solid state detector materials can be divided into compound materials, such as gallium arsenide, and single-element materials, such as silicon or germanium. Silicon is the dominant detecting material. Many of the other materials have their benefits, but in the end silicon is easily available at a decent price and in position sensing the other materials do not show clear benefits that would justify their usage, although single-crystal diamonds [18] are being studied because of their possible benefits in terms of radiation tolerance.

A silicon detector is not made of plain silicon. There is bulk doping of the order of 10^{13} cm^{-3} in the bulk. In addition, the terminals are doped to concentrations exceeding 10^{16} cm^{-3}, and therefore are orders of magnitude higher. The silicon detector is a diode: one of the terminals is n-type, the other is p-type. During operation the diode is reverse biased. There is a large electric

[1] A cautious reader might notice that the word *usually* is abundant in this text. This is since there are exceptions to almost all the statements made here. In this particular case, the detector material does not always have to be ionized to detect a particle when, eg., Cerenkov light or scintillation is used for detection. This footnote does not claim that there would not be ionization in those detectors, but it merely gives an example statement which is not strictly true but good enough in this context.

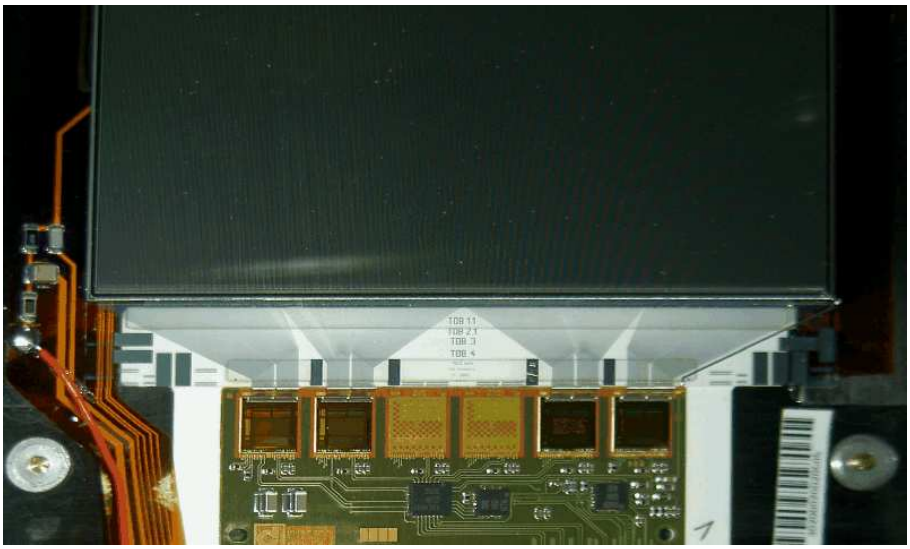

Figure 2.1: Illustration of a silicon strip detector (top) glued and bonded to readout chips (below) via a pitch adapter. This partially shown detector is a prototype of the barrel part of the tracker of the CMS experiment.

field, of the order of kV/mm inside the active material and almost no current flowing through the diode as it is reverse biased.

A simple and commonplace configuration is to segment one of the sides of the disk into many unidirectional strips (Fig. 2.1). Each strip acts as a separate sensor. Each individual read-out strip is connected to the bias voltage generator via a bias resistor (Figure 2.2). In addition, there are often [19] guard rings in the wafer surface around the active area of the sensor (Figure 2.2) to reduce the noise resulting from wafer edge currents. Sometimes the detector geometry is more complicated. It is possible to segment both sides of the detector [20, 21] or put terminals inside the bulk [22]. Non-unidirectional strips [23] and other geometries [24] have also been proposed.

A particle ionizes a fraction of the active volume of the silicon and leaves approx. 80 electron-hole pairs per μm behind. The acquired charge is collected to the terminals of the detector by the electric field created by the external bias. The most common particle detector is an n-type detector, where the p^+ terminal of the pn junction is segmented and used for position sensing, the bulk is n-type, e.g., doped with donors, and the backplane of the detector is n^+ doped. In an n-type detector, the backplane is more positive and holes are collected into the read-out strips. It is also possible to use the positive terminal for readout [25]. In p-type detectors the n-type strips collect electrons instead of holes, and compared to the more common n-type detectors the bulk doping and the direction of electric field are inverted.

While the charge is being drifted toward the detector surface, it also diffuses perpendicular to the plane due to Brownian motion. The magnetic field and tilt of the initial track can affect the shape of the acquired charge distribution. Capacitive coupling between the strips also affects the amount of charge present in nearby strips. Because of this capacitive coupling, not all strips need to be read out. Strips that are not read out are called intermediate strips [26]. Because of these effects, the induced charge can be shared to more than one read-out strip and the initial position of ionization can be interpolated and the resolution of the detector can be better than that suggested by the distance between read-out strips.

The moving charge carriers also induce crosstalk current to nearby strips by electric coupling [27]. This phenomenon could be used for data acquisition [28]. These signals sum to zero when integrated over the charge carrier drift time, and are not interesting in the applications discussed here.

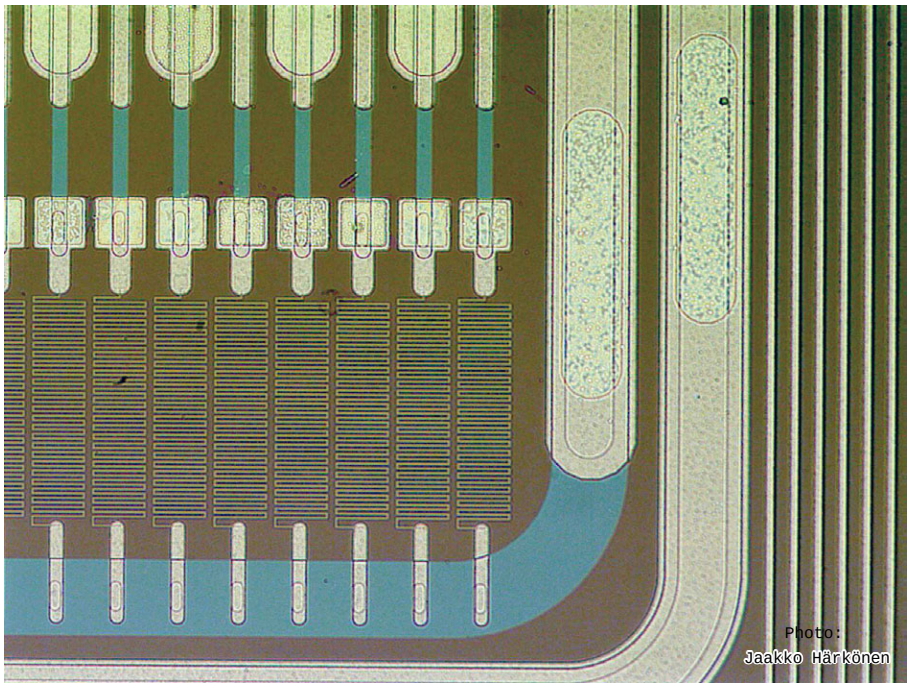

Figure 2.2: The corner of a silicon strip detector. Bias is fed from the bias ring via megaohm resistors. There are guard rings around the active area of the detector. The purpose of the guard rings is to absorb the leakage current at the detector edges. Square-shaped test pads are connected directly to the strips. The oval-shaped, interlaced pads are bonding pads. These pads are capacitively coupled to the strips collecting the charge [29].

In addition to the particle-induced signal discussed above, electron-hole pairs are also spontaneously generated in the detector material. This charge is collected by the detector and appears as Gaussian noise in the readout. The amount of pileup noise can be reduced by making the amplifier fast. However, increasing the amplifier speed without increasing the available power increases the noise in the amplifier. Therefore, the noise properties of the detector affect the requirements imposed on the read-out electronics.

The detectors studied in this work are 300 μm thick AC-coupled single-sided strip detectors. The processing of the detectors is described in [30]. Most of the detectors are made of n-type magnetic Czochralski silicon, though p-type detectors are also studied and detectors made of float zone silicon are studied for the sake of comparison [31]. The detectors have 768 strips with a pitch of 50 μm. The active area of the sensors is approx. $3.9 \times 3.9\,\mathrm{cm}^2$ [13].

Radiation damage

Radiation induces defects in the crystal lattice of a silicon detector. These defects modify the behavior of the detector in unfavorable ways. First, these defects can act as recombination centers that increase the leakage current and hence the noise. Second, the defects trap charge and hence reduce the charge collection efficiency, i.e. the signal. In addition to reducing the signal and increasing the noise, the defects also contribute to the effective space charge, which increases the operation voltage. The increasing depletion voltage and leakage current make stable operating conditions difficult to reach [32]. Irradiated detectors with n-type bulk doping undergo a type inversion, also called space charge sign inversion (SCSI). If such a detector is partially depleted, the low field region is found close to the read-out strips, which harms data taking.

One method for improving the radiation hardness of silicon devices is to incorporate oxygen

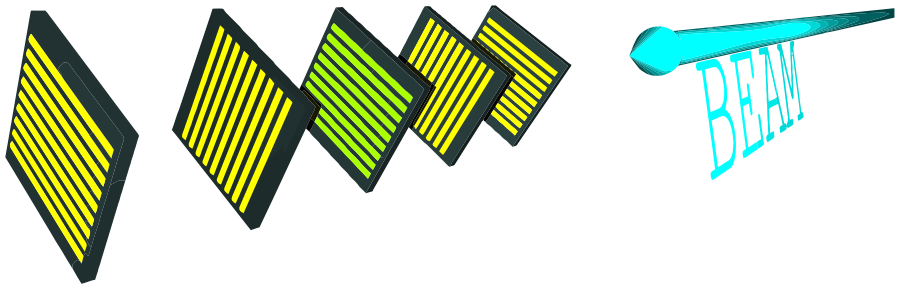

Figure 2.3: Simplified illustration of a beam telescope. Strip detectors and an arrow representing the collimated particle beam are shown. In the SiBT, the DUT's are located in the center of the telescope to minimize the impact point uncertainty of the reference track. Only four references and one DUT are drawn here for simplicity.

into the silicon lattice, because oxygen reacts beneficially with the radiation-induced defects, thus reducing the increase in the effective space charge concentration caused by the radiation [33]. Magnetic Czochralski detectors are being studied since the oxygen concentration of the material can be adjusted. Additionally, the material has sufficiently high resistivity and is also used outside the high-energy physics community and is commercially available at a competitive price.

In addition to material engineering, detector geometry engineering can also be used to tackle the problem [34].

Another method to improve the response of irradiated detectors is to use forward biasing to fill the above-mentioned traps together with a low temperature [35]. The low temperature facilitates keeping the traps full and reduces the bias current through the detector to a tolerable level. The filled traps modify the space charge of the detector bulk, which shapes the electrical field in a way favorable to particle detection [36].

2.2 A Beam Setup

In a beam test, a beam of particles can be extracted from a particle accelerator to form a tightly focused beam of particles with a well defined momentum and type [37]. These particles can be delivered to a beam test setup to measure the response of particle detectors under test in controlled conditions. The beam particles used are minimum ionizing particles, i.e., the energy loss of the beam particles (dE/dx) resembles those that will be of interest in the HEP experiments, too (Ch. 27 of [38]). The beam tests described in this study have been carried out at the H2 beamline at CERN Prévessing site, 225 GeV pions being the preferred test particles.

A beam setup contains layers of reference sensors, which are used to reconstruct the reference tracks. In the beam setups that are discussed here the detectors are in succession, and each beam particle passes through all the reference detectors. The reference detectors are single-sided silicon strip detectors. As such detectors do not measure the particle location in the direction of the strips, the direction of the strips must be altered from layer to layer to obtain positional information in all co-ordinates. Figure 2.3 contains a simplified picture of a beam setup with five layers. The devices under test are usually located in the center of the telescope, where the positional uncertainty of the beam particle tracks is at minimum.

The silicon detectors must be located in a light-tight container when in use. It is sometimes beneficial to be able to control the ambient temperature and humidity of the detectors. It would also be beneficial to be able to rotate the detectors when needed. Photographs of the actual setups can be found in Figures 3.6, 3.7 and 6.1 on pages 15, 16 & 36. A beam test setup includes a trigger system, which detects the arrival of the beam particles. One event is recorded whenever an

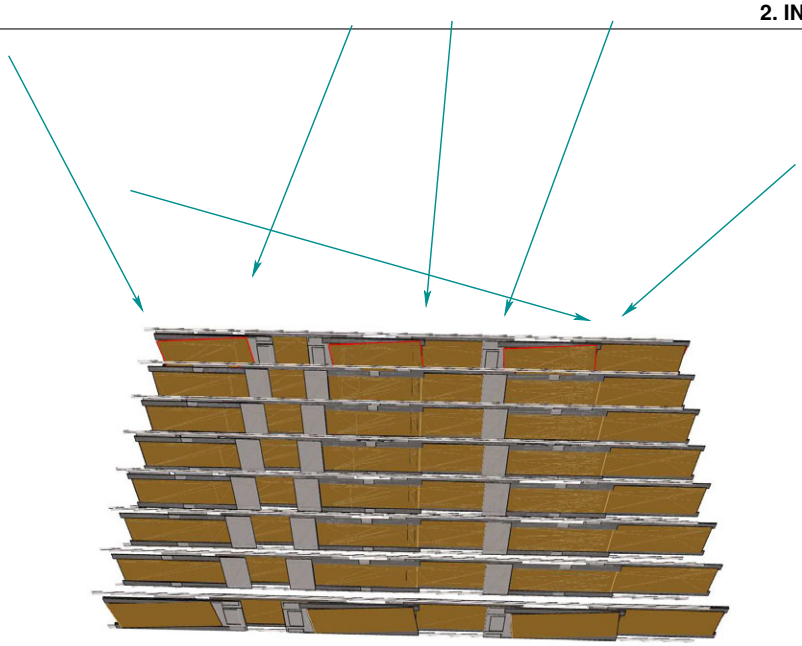

Figure 2.4: In a cosmic setup, the particles arrive from all directions. This figure illustrates the positioning of the FinnCRack detectors. In FinnCRack, the detectors and associated electronics are located in so-called rods. The rods used at FinnCRack are prototype rods of the outer barrel part of the CMS tracker discussed in, e.g., [39].

arrival particle is detected by the trigger system, unless the particle is vetoed. A typical reason for vetoing a trigger would be that the readout system is busy processing the previous event.

Beam tests are also used to characterize other types of detectors in addition to those discussed here.

Cosmic setup

It is also possible to use cosmic particles instead of accelerator generated ones. The main differences between these options are listed below:

- Particle beam availability is often limited, while cosmic particles are always available.
- The energy and type of particles in a beam can be chosen within the constraints of the accelerator. Cosmic rays cannot be manipulated.
- The time of arrival of a beam particle can be known in advance; cosmic particles cannot be predicted in this way.
- The particles of a beam are collimated. Cosmic particles have a large angular and positional spread.
- The intensity of the beam setup can be chosen. The cosmic rays arrive at a pre-determined rate of approx. $90\,\mathrm{m^{-2}s^{-1}}$ [38]. Only a fraction of the cosmic rays can be measured as a result of the angular acceptance of the setup, and the possible usage of timing and energy filters.

The cosmic particle rack discussed in this work is called FinnCRack. The name was chosen to avoid ambiguity since a similar telescope has also been constructed at CERN. Some detectors are placed side-by-side to compensate for the large angular spread of the cosmic particles (Fig. 2.4).

Chapter 3

Data Acquisition

This chapter briefly describes the electronics needed to read out a silicon detector. The focus is tightly on the high-energy physics-oriented read-out systems described in the attached articles; there are a number of other position-sensitive silicon detectors, such as those of a digital cameras, which are not discussed here. First, the vital data acquisition components are discussed; practical details of the actual apparatus are discussed at the end of this chapter.

The radiation hardness of the front-end electronics is an important question for future high-energy physics experiments. The methods used to improve the radiation hardness of the electronics are different from those of the sensors and are studied separately. These issues have been avoided in this study by bonding the read-out chips to the sensors after irradiation, and hence the radiation hardness of the electronics is not discussed here.

3.1 Readout chip

When a minimum ionizing particle (MIP) penetrates a silicon detector, it generates a trail of electron-hole–pairs along the path of the particle. Approximately 24 000 electrons are collected by a good-quality fully depleted 300 μm thick sensor in a typical event. The speed of the charge collection depends on, eg., the bias voltage and detector geometry, and is typically around 100 μm/ns. The majority of the signal is seen within nanoseconds [40]. After being collected to the strips, this signal slowly fades away (Fig. 3.1).

The strip is typically capacitively connected to a charge-sensitive amplifier. The speed of this amplifier is important for the performance of the system. All detectors produce noise in addition to a signal. The noise causes the amount of charge seen in the amplifier input to vary randomly. A noisy detector requires a fast amplifier to reduce this white noise. A fast amplifier is, however, noisier than a slow amplifier. For the best results, the characteristics of the amplifier should match those of the detector [41].

After amplification the signal goes through a pulse shaper. The output of the shaper needs to be sampled at the correct point of time. There are some approaches to address this:

- The simple solution used, e.g., by the VA1 chip [42] of SiBT99, stores the sample into an analog sample-and-hold circuit whenever the trigger (p. 8) arrives. This method requires the response time of the trigger system to match the time constants of the preamplifier and shaper. If the time constants are short, this might not be an option.
- The output of the shaper can be compared to a set threshold and the result of the comparison can then be stored. This approach is used mainly with a digital readout.

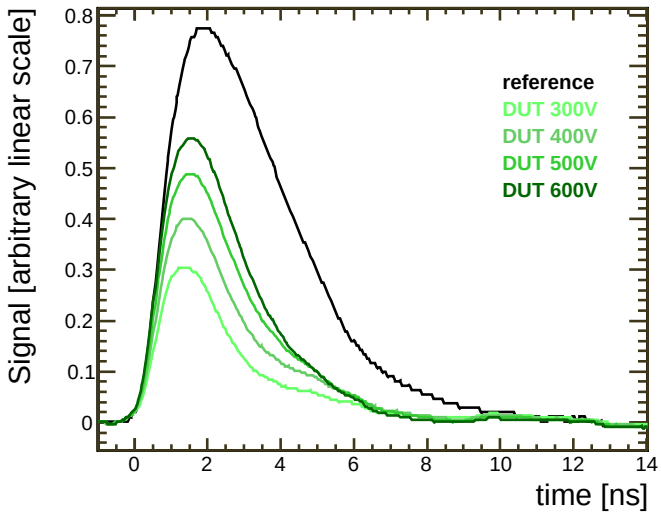

Figure 3.1: Signal response to and infrared laser pulse of a reference diode and an irradiated silicon test diode (being underdepleted) at various bias voltages measured using a TCT setup [46]. Typical pulses will be longer at the output of the shaper of the readout chip.

- In the time over threshold method [43] the output of a shaper is compared to a predefined constant, and the resulting bit is periodically fed into a shift register. The number of bits in the register contain the charge information. The scale is, however, not linear and is approximately logarithmic. The comparator and the shift register must be clocked at a speed which is fast compared to the analog time constants described above.

- The output of the shaper can also be periodically stored to the analog memory, which can be used to increase the time available for triggering. The APV25 chips [44] used in SiBT07 and FinnCRack utilize this method.

  Using a synchronous chip in asynchronous conditions leads to excess jitter [45] in the timing of the chip trigger, as the sampling takes place before the time of arrival of the particle is known. This converts into a loss of signal, as the optimal sampling point is frequently missed. If this is a problem and there is no need to store all the triggers, the issue could be partially solved by actually sending the trigger to the front-end chip only when the trigger timing is close enough to an actual sampling point.

The study of DUT properties is straightforward when the readout system delivers the analog, linear response of the devices under test. Both the VA1 and APV25 chips used here fall into this category. Other types of chips are mentioned for the sake of curiosity only.

The measurement data must be transmitted out of the chip. A common approach that is used in all the chips used in this work is to serialize an event, i.e., transmit all the analog samples away one by one.

The output of the asynchronous VA1 chip [42] is clocked externally. The token bits that select the output channel must be fed to the chip separately. In the absence of a token, the VA1 outputs are in a high-impedance state. This allows several chips to be read out through one serial line. In the APV25 chip [44] of the CMS the measurement signals are also output serially. Unlike in VA1, the order of the data in APV25 is non-consecutive [47]. This makes it possible to perform a separate study of the correlations in the adjacent strip data and the correlation of subsequent samples caused by the characteristics of analog transmission path. The APV25 packets comprise synchronization bits, a digital header identifying the chip state at trigger followed by the analog

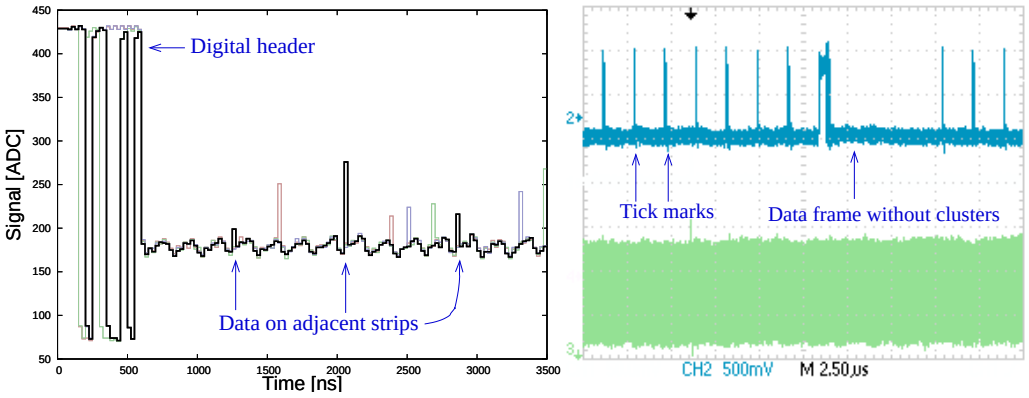

Figure 3.2: The APV25 chip outputs its data in frames containing a digital header and analog measurement data (left). Four separate frames are show, one being emphasized for clarity. When there are no data to transmit, the chip periodically outputs synchronization marks called tick marks (right).

samples. Both VA1 and APV25 packet lengths have a fixed length. The output of the APV chip is shown in Fig. 3.2.

Chips doing data reduction must have a more complex data format. For example, the ABCD3TA chip [48] used in ATLAS [49] compresses the data by sending the strip addresses of strips with a signal above a threshold and in addition it indicates that the next strip was hit too by applying only a single bit to the output stream. It also used daisy-chaining in order to fully benefit from the variations in data packed lengths from chip to chip. In the possible future upgrade of the SiBT, it would expand the possible uses of the device if the apparatus is designed in a way which allows the easy digesting of the data format of other readout chips when a need to read out those chips arises.

3.2 Supporting electronics

Readout chips need to be configured. The configuration of the analog part of the chip could be implemented, e.g., via bias currents generated outside the chip (VA1 way) by supporting electronics or via in-chip bias generators. In the latter case, the chip is initialized digitally, e.g., via the I^2C bus in the case of the APV25 chip. The biases typically: 1) affect the gain of the system; 2) keep the signal in the linear range of the analog transmission path, and 3) affect timing. As even a simple beam test setup contains dozens of readout chips or more, the ability to control these bias currents remotely in a centralized manner is beneficial in system commissioning and debugging.

The purpose of the rest of the readout chain is to transmit the signal to the analog-to-digital converter (ADC) with minimal losses in signal quality. To maintain a good signal quality, it is most important to avoid excess noise in the analog data. Some common sources of noise are listed below.

- Noise in the bias voltage of the detector is picked up by the detector and translates into excess noise in the measurement data.
- Ambient electrical noise is picked by the detector or one of the components of the transmission path. The effect of noise picked by the transmission path on the data quality can be reduced by amplifying the signal early on; the removal of the possible sources of such noise helps too.

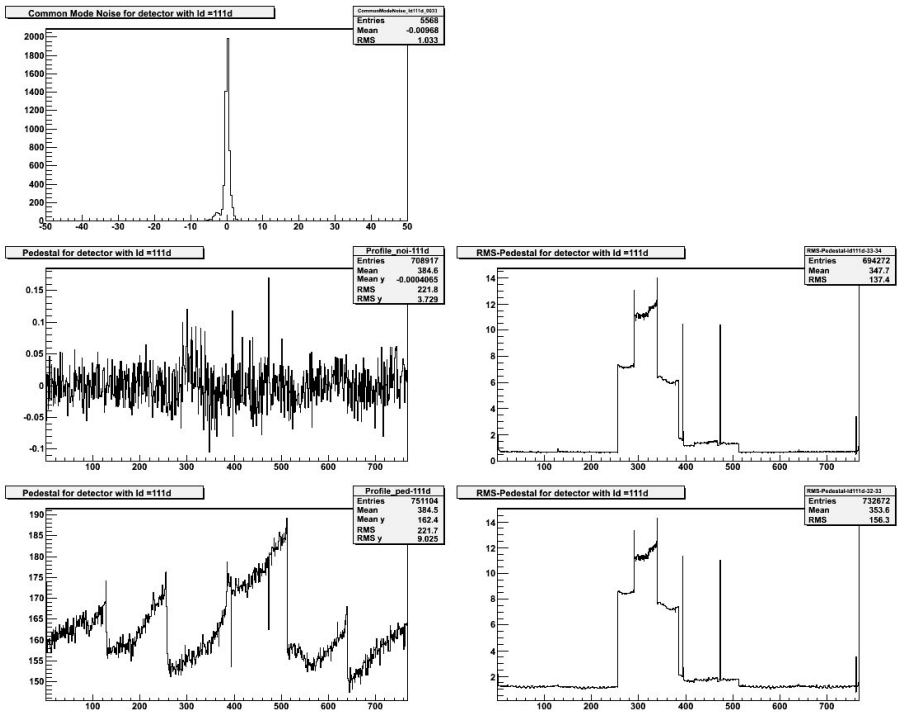

Figure 3.3: Authentic online performance plots of SiBT07 depicting data while they are being acquired. The same data are plotted from various points of view. Analysis details are discussed in Chapter 4. The plots on the left show common-mode (CMN), pedestal-subtracted pedestals and raw pedestal values (p. 18). Raw and CMN-subtracted noises are shown on the right (p. 19). Interpreting these plots is not always straightforward. In this particular case, two mini-sensors are being characterized.

- Noise in the power fed to the read-out electronics leaks to the measurement data. A wrong voltage level can also show up in this way. The noise in these inlets could originate from the power supply itself or could also be picked-up ambient noise.

Errors committed in biasing the system, and especially timing problems, such as ADC sampling its inputs during the transition phase, can also appear as excess noise.

The signal levels output by the readout chip are rather small, few centivolts for VA1. In the case of APV25 the data are also unipolar. Amplifying the signal in the vicinity of the readout chip and transmitting it forward as a differential signal reduces the noise pick-up.

When interpreting the test results, it is usually important to know under which conditions the test was done. The number that is acquired is often compared to another one, e.g., the signal value of a novel detector is compared to that of a well-known one. Such a comparison makes sense only if both measurements are carried out in the same way. If there are many factors affecting the measurement result, it would no longer be possible to conclude whether the DUT differs from the standard detector in the expected way as the differences seen could be explained using other means too. As an example, if the voltage dependence of the noise is being measured, it is important to monitor the temperature of the device under test since the noise could also depend on temperature. The reliability of a measurement where some of the important parameters remain unknown would be questionable.

To achieve reliable measurement results in this manner, it is beneficial to monitor and log the important environmental factors affecting the measurement result. Having a good monitoring system speeds up the measurement apparatus assembly, too, by speeding up the debugging

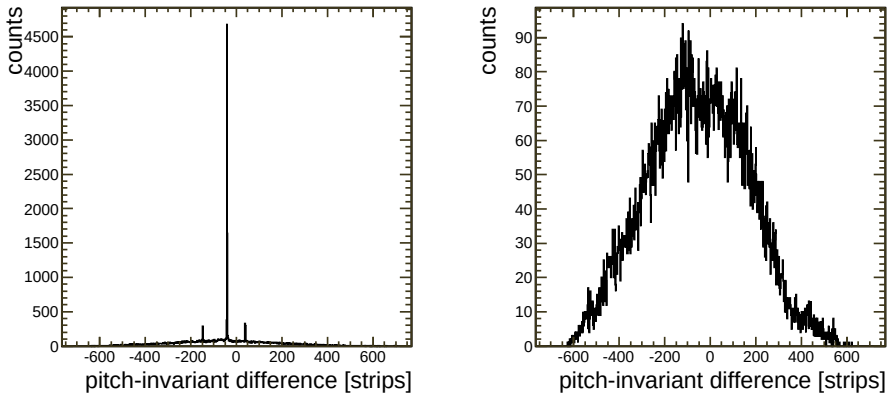

Figure 3.4: Correlation plot: for each event, the strip number of each cluster in one reference detector is subtracted from the strip number of each cluster in a DUT detector and a histogram is produced out of these differences (left). A similar histogram made out of the same clusters is shown on the right. In the left-hand histogram, each cluster pairs is formed from one event; on the right, there is an intentional offset in event numbers between the detectors. Correlations between Detectors 0 and 3 (see page 33) are shown.

phase. The measurement results should be logged since there can be issues in the data that could be explained by environmental factors that are not detected during data taking. Not having logs forces data analyzers to speculate about the actual course of actions.

Sometimes the device under test needs to be read out using electronics different from those used by the reference apparatus. When this is the case, the read-out systems need to be merged. When that is not feasible, then the triggering of the two systems must be done in such a way that the data of the two systems can be united later. One way to achieve this is to use a common trigger system and ensure that all triggers are accepted by both systems. This approach is rather straightforward if there is an easy way to ensure that the trigger system is aware of the dead-times of both systems. Another way is to associate a unique identifier with each trigger and make both systems attach those identifiers to the respective measurement data.

Online data processing

The purpose of online data processing is to ensure that the measurement system works properly and that it is properly tuned. All the telescopes discussed in this work utilize online monitoring.

In online monitoring, the data are visualized (Fig. 3.3) while being acquired. This provides a quick feedback loop and allows the operator to notice a large number of potential problems, such as if a detector is not biased or the connection between the detector and the readout is lost.

The SiBT07 apparatus utilizes quasi-online analysis in addition to online monitoring. In quasi-online analysis, recently written data are read from the disk and analyzed. This method produces more delay compared to online analysis, but it has the potential to discover problems not seen by online monitoring for two reasons: 1) it will capture corruption problems that occur in the data path after the online monitoring tool has copied the data. A disk-full situation would be one example of such a problem; 2) the analysis software can run more complex analysis on the data, which allows it to notice a larger number of problems. If this quasi-online analysis produces the expected results, it is likely that the more detailed analyses carried out later will also be able to digest the data files.

An example quasi-online plot is shown in Figure 3.4. A peak in the histogram demonstrates that a cluster in one detector can predict the position of a cluster in another detector. The correlation is caused by the primary beam and the peak is a demonstration that the detectors respond

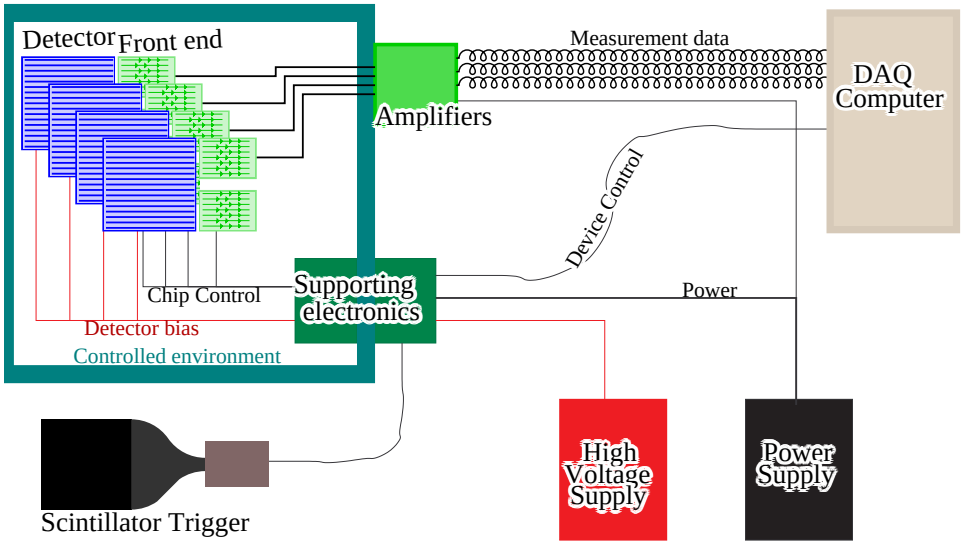

Figure 3.5: A schematic diagram showing the main components of the particle telescopes. The preamplifier, shaper, analog memory, and multiplexer discussed in the text are part of the front-end chip. A fraction of the supporting electronics is usually located at the front-end hybrids housing the read-out chips. See pages 5 and 15 for photographs of the hybrids.

to the beam. The position of the correlation can be used to check that the detectors are (roughly) aligned. This kind of histogram is easy to produce, but it requires the direction of the particles that are arriving to be known in advance. The control measurement also shown in Figure 3.4 excludes the possibility of the peak that is seen being caused by clusters constructed around noisy strips. The fact that the correlation peak differs between these two plots reduces the possibility of the peak that is seen being an artifact. However, these particular plots do not rule out the possibility of the peak being caused by cross-talk between readout channels.

During data taking, it is important to be aware of the potential problems that are not revealed by the monitoring tools in use, especially if data are being discarded on-line.

3.3 Measurement apparatus

Three separate measurement systems are described in the attached articles: **[I]** describes the Silicon Beam Telescope (SiBT99); **[III]** describes the upgraded telescope (SiBT07) and article **[II]** describes the Finnish Cosmic Rack (FinnCRack) apparatus. The main components of the apparatuses are described below and depicted in Figure 3.5.

SiBT99 uses a VA1 [42] based readout. Each detector module is housed in its own light-tight container (Fig. 3.6). Scintillators and so-called repeater cards that amplify the signal and provide readout chip biases are also placed in the beam area. All the chips of one detector are daisy-chained for readout and all detectors receive the same trigger and clock information from the device control, which reduces the amount of cables needed between the beam area and operator premises. The calculation takes place in a VME rack, which can be placed several dozen meters away from the measurement apparatus itself. The device is rather compact (Fig. 3.6).

Unlike SiBT99, SiBT07 and FinnCRack utilize APV25 [44] chips. The front-end of the APV25 chip is fast compared to that of the VA1 and therefore is better suited to the study of noisy detectors. The APV25 is synchronous (VA1 is not), which complicates either the data taking or the data analysis. The chip is built with LHC experiments in mind. Neither the H2 beam of SiBT07 nor

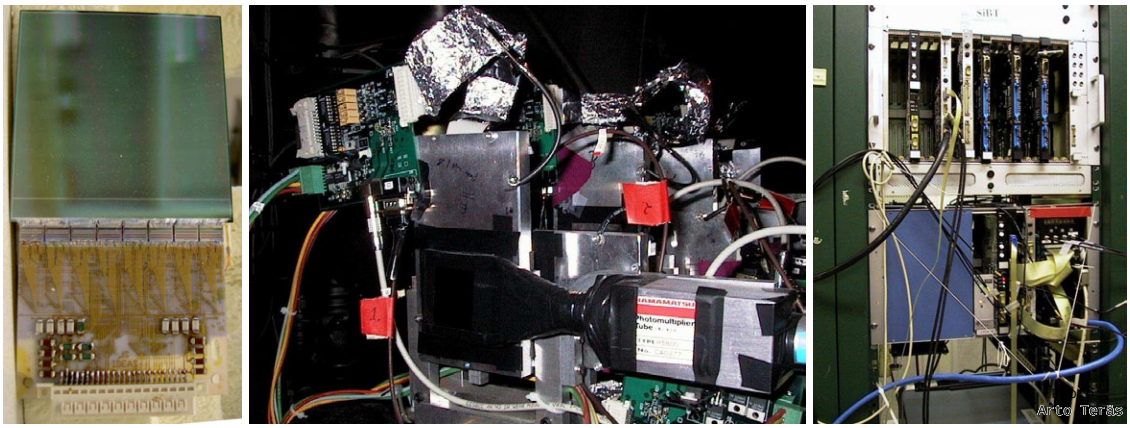

Figure 3.6: The SiBT99 apparatus. Each detector module (left) is housed in its own light-tight container (center). The read-out electronics fit into one VME crate (right).

the cosmic particles are synchronized to the master clock of the measurement apparatus. Therefore, either a trigger is assigned to the closest clock cycle or triggers are vetoed on the basis of the phase of the clock. The former causes a fraction of the data to be sampled at a suboptimal point of time, and the latter reduces the data rate. The devices are capable of both approaches, but so far data quantity has been preferred over quality. In the case of FinnCRack the decision was made because of the already-low trigger rate, and in the case of SiBT07 the decision was made in order to minimize the amount of beam time used to calibrate the SiBT07 itself.

In SiBT07, the detector modules are built on top of plug-in modules that can be quickly inserted into a temperature-controllable container called the Vienna box (see Fig. 6.1 on p. 36). The readout is implemented in the PMC modules, which are inserted into normal office PC's in the vicinity of the Vienna box. The amount of equipment and surface area needed by SiBT07 installation is large compared to the size of the Vienna box itself. This also slows down the installation of SiBT07. The Vienna box can be utilized at temperatures above -25 °C. The lower limit is set by the cooling power of the Peltier elements used and the amount of heat generated by the readout electronics when in use. If lower temperatures are needed, an additional Coldfinger box has been constructed for SiBT07 use. This uses a three-stage Peltier element to cool the detector. The lowest temperature achieved with this setup is -53 °C.

There are so-called Vutri cards attached to the backplane of the Vienna box. These amplify the measurement data from the chip and convert them to differential form. They also regulate the voltages to the readout chips. In the SiBT99 the corresponding boards are called Repeater cards. In FinnCRack, the conversion of the signal from electrical to optical form takes place in the rods (see below), making the length of the analog electrical data path only a few centimeters long.

The FinnCRack detectors (Fig. 2.1) are merged into superstructures called rods (Fig. 3.7) which provide mechanical support and cooling and house additional electronics for optical data transmission, chip calibration and monitoring of the environment. The rods of FinnCRack are similar to those used in the outer barrel part of the CMS tracker. FinnCRack is placed into a cold chamber when in operation. In Fig. 3.7 FinnCRack is shown in front of its cold chamber. The communication between the rods inside FinnCRack and the data-acquisition back-end happens using optical fibers. The distance between these two can be large. In FinnCRack, the ambient temperature control is separated from the cooling of the rod components [50]. Temperature, humidity and coolant flow monitoring are completely separated from the control, both in FinnCRack and SiBT07.

Each SiBT99 detector is housed in its own light-tight container, which is not temperature controlled. When there is a need to lower the temperature, it is possible to replace one of the containers with a "cold box". Humidity is controlled with an adjustable nitrogen flow in the Vienna box of SiBT07 and the cold box of SiBT99 and using an air drier (Donaldson ultrapac

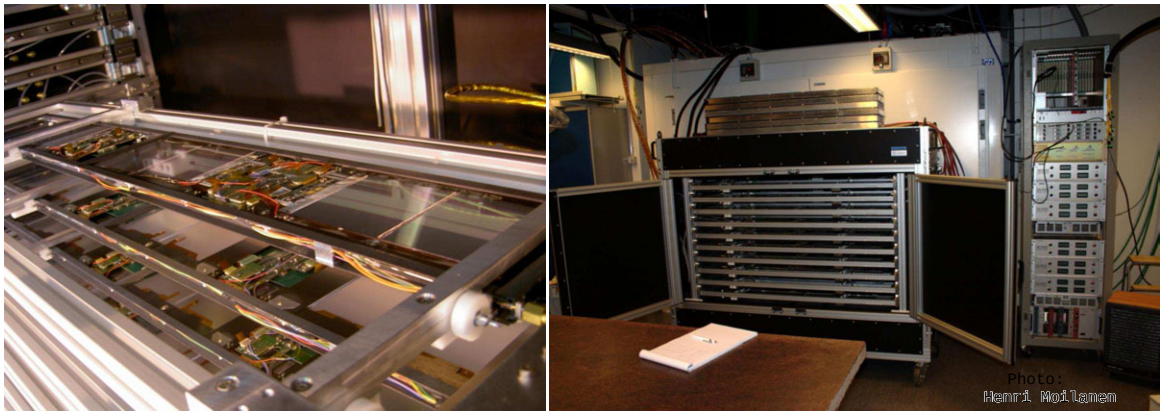

Figure 3.7: The FinnCRack apparatus. The detectors (Fig. 2.1) are merged into superstructures called rods (left). FinnCRack itself is in front of its cold chamber (right).

2000) in FinnCRack and hermetic sealing together with silica gel in the case of the SiBT07 cold box.

The triggering of the measurement system, i.e., observing the arrival of the particles is done using scintillators and coincidence units that produce a trigger only when all the sensors see the arriving particle within a set time window. SiBT07 and FinnCRack are able to discriminate between the triggers on the basis of the phase of the 40 MHz system clock, in 1 ns resolution. The large 1.4 m-long scintillating plates used in FinnCRack trigger have a high refractive index (1.6). This leads to a large uncertainty in trigger timing that needs to be compensated. One way to reduce the jitter is to benefit from the fact that there are photomultipliers at both ends of the scintillators. Averaging the arrival times of the trigger pulses reduces timing uncertainties associated with the length of the scintillators. It might be possible to extract positional information from the time differences to further improve the apparatus.

The data of the read-out chips are amplified in all the setups and then transmitted to an analog-to-digital converter (ADC). In FinnCRack, data are transmitted between the front-end and read-out using optical fibers; in the other system the signal stays in electrical form throughout the analog path. The use of fibers reduces the risk of noise pick-up. Each fiber has its own analog gain, which must be taken into account and which therefore adds some uncertainty to the absolute value of the signal strength. The ADC linear ranges are 12 bits (ROxi [51] of SiBT99), 9 bits (FEDPMC [52] of SiBT07) and 10 bits (FED9U [53] of FinnCRack) wide.

The SiBT99 readout performs the online clusterization of data. Pedestal and noise levels are updated continuously using the exponentially moving average algorithm (EMA). The clusterizer accepts strips where the signal and signal-to-noise ratio are above a threshold. Immediate neighbors of such strips are also accepted. The clusters are then written to disk. In addition to the signal, an SiBT99 cluster also carries information about the noise. FinnCRack is also capable of online clustering. In the case of FinnCRack, a cluster only contains the cluster signal; the pedestal and noise must be calibrated in separate pedestal runs if online clustering is used. To facilitate the analysis, FinnCRack has thus far never been run with on-line data reduction activated. SiBT07 does not have on-line clustering as an option.

The SiBT99 read-out hardware is designed for that particular device, and comprises VME6U boards digitizing and clustering the data. The data are then passed to storage via the VME bus. SiBT07 is built on top of old CMS prototype boards, which are PCI Mezzanine Cards which are housed inside normal office PCs [52, 54]. That of FinnCRack is done using more recent versions of CMS prototype boards. The FED9U read-out cards of FinnCRack feed their data to the VME bus.

The VA1 chip calibration in SiBT99 is performed using trimmers, and the bias points are

searched manually, using an oscilloscope and a screwdriver. The APV25 chips are biased digitally using the front-end controller (FEC) board [55], which talks to several communication modules (CCU) [56] using a token-ring like protocol. The CCU modules then relay the information to the chips via the I^2C bus. The latter approach is initially more time-consuming to set up, but the calibration itself is fast, easy to carry out, and less prone to human errors.

The online data acquisition software of SiBT07 is based on the December 2005 version of the corresponding CMS software [57]. The reason for using such an old version is the compatibility with the old hardware. The quasi-online analysis is based on the CMS analysis software (Section 2.2 of [8]). Several modifications have been made to both software packages to make them better suited for SiBT use. FinnCRack uses CMS software based data acquisition and analysis similar to those of SiBT07 and one described in [58]. The SiBT99 software does not have a common ancestor with the other two setups.

Chapter 4

Data Analysis

The objectives of test beam data analysis are to reconstruct the measured events and use the reconstructed data to obtain the properties of the device under test.

Throughout this chapter, the assumption is made that the data to be measured have been recorded using a linear analog read-out that does not do any on-line data reduction. In other words, some SiBT99 issues are skipped in order to simplify the text.

The beginning of this chapter describes how the event is reconstructed. Then the focus moves to the analysis of the device under test. These are handled separately to emphasize that mixing the reference data and the measurement data should be done with care.

4.1 Reconstruction

The data seen by the read-out are a superposition of the actual signal, detector noise, and readout noise. The sections below describe the steps needed to reconstruct the event, and also describe some quantities that are interesting when the performance of the device under test is evaluated.

Pedestal

There is typically a constant offset in the raw analog data, called the pedestal. The existence of the pedestal is due to the need to ensure that the output signal of the read-out chip remains in the linear range of the read-out electronics. One of the first steps in the analysis is to subtract the pedestal; in other words, to bring the gauge to zero when there is no signal.

A straightforward approach to pedestal correction is to calculate the mean value of each read-out channel for an entire run, and use that as a pedestal which is then subtracted from the raw data in pedestal subtraction.

The signals from particles being measured can make the pedestal values calculated using the straightforward approach appear higher than what the true pedestal is. This possible bias can be reduced by calculating a median value instead of a mean value. The bias can also be reduced by excluding the clusters (see below) in pedestal calculation. Cluster removal requires the clusters to be identified, which in turn can only be done after pedestal calculation. This leads to pedestal calculation being iterative. It also introduces possible biases to the calculated pedestal value caused by a failure to exclude a genuine cluster and the accidental removal of a fraction of noise as a result of it being misidentified as a cluster.

Another method to remove the possible bias caused by particles being measured during pedestal calculation is to ensure the absence of particles. This can be done, e.g., by separate

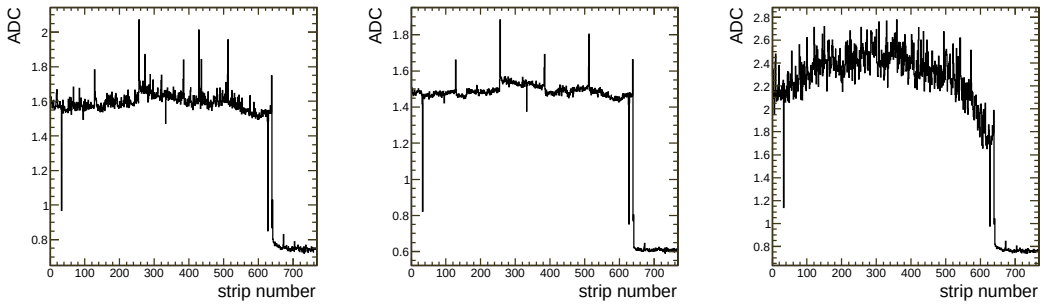

Figure 4.1: Noise plots. Raw noise (left) and common-mode subtracted noise (center) calculated with cluster exclusion algorithm and raw noise (right) calculated without cluster exclusion. The noise values are standard deviations as described in the text, plotted separately for each strip in analog-to-digital converter units (ADC). The same dataset was used to generate all these plots. The data of Detector 0 (see page 33) are shown. Detector 0 has 639 strips instead of 768 as the devices under test do; the last read-out channels are floating.

pedestal runs, where the data acquisition system is operated in the absence of real particles. This method avoids errors in pedestal calculation that are caused by problems in the cluster exclusion, since no cluster exclusion is needed.

The pedestal values depend on external conditions, such as temperature, humidity, and operating voltages. These dependencies are usually not well known. The aim is to keep operational conditions stable, but nevertheless the measured pedestal values are valid only for a limited period of time. In short, pedestal runs need to be re-run periodically. Frequent pedestal runs provide information on the stability of the measurement system. The possible errors in pedestals caused by temporal offset can be avoided by using the data of the same run instead of a separate pedestal run. It is possible to reduce the contamination of a particle-induced signal in pedestal calculation, and avoid the possible error resulting from the removal of entries that are actually noise by first reconstructing the tracks and then using the vicinity of a reconstructed track to indicate the existence of a particle-induced signal in the calculation of pedestal values. This method works only when one can be certain that there are no missed tracks in the data being re-analyzed.

It is usually assumed that the operating conditions do not change inside a run. Sometimes a common mode (see below) distribution that is not centered around zero (Figure 3.3) can be used to indicate the use of ill-suited values in pedestal subtraction. In SiBT99 analysis the assumption of constant pedestal values is replaced with the assumption that pedestal values are drifting slowly, and the pedestals are constantly updated during data taking. This approach reduces the risk of the data acquired being biased as a result of the use of wrong pedestal values.

Noise

The noise can be sub-divided into common mode noise and readout channel noise.

The common mode noise is the noise component that is common to many read-out channels in a single event. Common sources of common mode noise could be the mains phase picked by the detector and ripple in the operating voltage of the read-out chip. The common mode should, by definition, be calculated for a large number of strips. For practical reasons[1] it should, however, be calculated separately for each read-out chip, and in the event that not all the channels of that chip are connected to the same detector, then the common mode calculation should be further divided into groups of strips on the basis of where they are connected to. Strips that contain

[1]The read-out chips can pick common mode, too. There is no guarantee that all chips will pick the noise similarly.

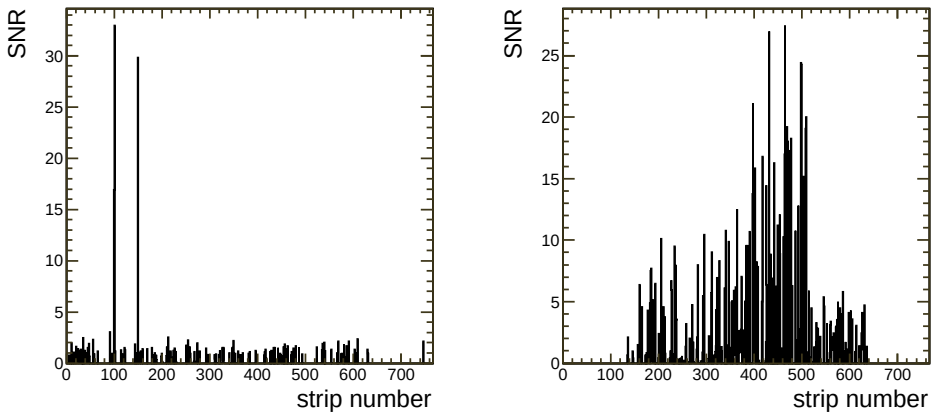

Figure 4.2: Zero-suppressed signal to noise ratios of one event, plotted separately for each strip. The data of Detectors 0 (left) and 3 (right) are shown. Usually, there is one real cluster present in an event. It is unlikely that all the clusters present in the Detector 3 data would be responses to beam particles. The detector numbering is described on page 33.

particle-induced signals and non-working strips (p.25) should be excluded from the calculation of common mode noise (Fig. 4.1). Since the common mode is a value specific to each event, it must also be calculated during data taking and therefore separate pedestal runs cannot be used to circumvent the cluster-exclusion issue. As the location of clusters is typically not known during pedestal subtraction, the pedantic analysis of an event is an iterative process.

The simple case is when the common mode is constant in space. In other words, all the read-out channels see the same phase and amplitude of this noise component. In this case the common mode can be calculated as a median of pedestal-subtracted signals of participating strips.

Channel noise is noise that is specific to each read-out channel, and is introduced to the system both by the detector and the read-out system. Often it is safe to assume that these sources of error follow the Gaussian distribution. The noise level is calculated separately for each read-out channel, e.g., as a standard deviation of the common mode subtracted raw data. If separate pedestal runs are not being used, then the exclusion of particle-induced signals needs to be implemented (Fig. 4.1). Noise calculated without common mode subtraction is called raw noise.

There can be event-by-event correlations of channel noises as a result of, e.g., capacitive coupling in the detector and cross-talk in the read-out chips and finite bandwidth in the amplifiers of the serialized data in the analog read-out chain prior to digitization.

Clustering

In clustering, the measurement data are splitted into segments containing interesting parts of the data. The purpose is to isolate those strips that contain information relevant to the measurement of the particle position.

The traditional method of clustering is to first calculate the pedestal and noise levels of each strip; when these are known, the measurement data are re-evaluated event by event, the common mode correction is obtained, and then for each strip its pedestal and associated common mode values are subtracted from the raw data. Data handled in this way are called strip signals here. Then for each strip, the ratio between the strip signal and strip noise is studied (Fig. 4.2), and clusters are formed according to clustering thresholds. A simple clustering method could be, e.g., to form a cluster of a contiguous set of strips that have not been invalidated and all have a signal to noise ratio (SNR) above a set threshold. In the SiBT99 the immediate neighbors of such strips were accepted regardless, of their SNR.

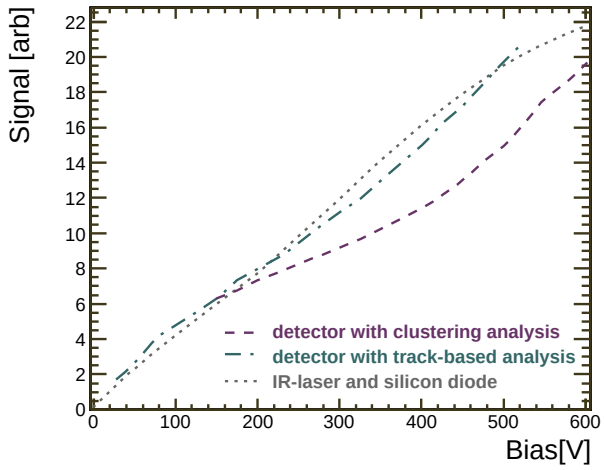

Figure 4.3: Comparison of signal vs. bias voltage plots using various methods. The data of Detector 7 (see p. 33) and scaled data of an MCz diode irradiated to the same fluence are shown.

There are many more complex clustering methods in use. In the CMS, first the data acquisition system reduces data with an algorithm where the acceptance of a strip depends on the charge of that strip and of the charge of the four adjacent strips and a total of two separate discrimination levels, leading to entities called *Digis*. During high-level triggering and analysis these digis are then fed to a clusterizer that uses SNR values and a three-threshold algorithm to construct the actual clusters. In the case of the CMS, the clusters can also be wide, and the simple approach quoted earlier would not work well. The two-step process of producing *Digis* out of *RawDigis* online and clustering the *Digis* later is a good way to handle the amount of data present in the CMS tracker (p. 3).

The clusters can later be divided into track-associated and non-track-associated clusters using a residual cut, i.e., based on how far the cluster centroid (see below) is from the track impact point. Non-track-associated clusters[2] are often called noise clusters. If the detector were used in track building itself, a similar classification would follow via track pattern recognizing.

Track-induced clustering

In track-induced clustering, the cluster is defined as comprising the strips in the vicinity of a reference track projected onto the detector surface. Track-induced clustering therefore requires the track position to be known and is not well suited for cluster formation in all of the detectors. If the error in the track position is not negligible, the width of the cluster must be chosen in such a manner that the strips carrying a large enough fraction of the total collected charge are included into the cluster with a high enough probability. The definitions of "large enough" and "high enough" above depend on the goals of the research being carried out.

If the track error is small compared to one unit cell in the detector, then the cluster width can be chosen to be such that the clusters resemble those acquired using SNR-based methods. If this is done correctly, the acquired cluster signals are comparable to those of the traditional methods, with the exception that the possible bias caused by the fact that only a subset of the actual detector responses to particle-induced signal, namely those that pass the SNR cut, are included. If the cluster size is set to be wide, then a larger fraction of the total collected charge is seen. These results are not directly comparable to traditional clustering results, but they compare

[2] All clusters with a particle-induced signal are track-associated only if the reference system reliably finds all particles.

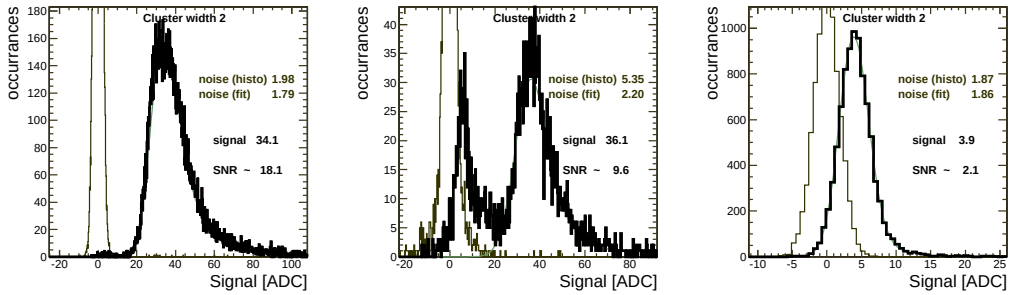

Figure 4.4: Signal histograms acquired using track-induced clustering. The control measurement is also shown. Noise data attached to the plots are calculated as RMS and function fit sigma of the control measurement. The data of Detectors 0, 3 and 11 (see p. 33) are shown.

well to those obtained using measurements from a non-segmented detector. In other words, this allows a comparison of the diode test results with those acquired using a real strip detector (Fig. 4.3).

The track-based analysis allows another straightforward method to cross-check that the signal that is acquired actually reflects the detector response to the particle being measured. In the control measurement, clusters are formed as in track-induced clustering, with the exception that the cluster of each event is formed around the impact point of the track of the following event[3]. In short, the DUT and reference data have an offset in their event numbers. Plots produced in this way will have the same beam profile and have the same amount of entries and are measured at the same time as the track-induced clustering data. Differences in track-induced clustering results and corresponding control measurement results are a strong indication of the genuine detector response to the particle being measured (Fig. 4.4).

Hit point assignment

The next step in the reconstruction chain is the hit point assignment. In this step, the hit position, as seen by the detector, is calculated from the data of a cluster. Some hit point assignment algorithms can also estimate the precision of the acquired hit point.

In the center-of-gravity (CoG) method, the hit position is calculated as the mean of the strip positions, weighted with the signal values of the strips. The CoG method works in a large number of use cases. The reported precision of the measurement is sometimes scaled with the cluster width. The aim in usually to reconstruct the hits with a precision better than the digital resolution. In CoG, the effect of noise on the strips far away from the center is emphasized because of the lever arm. Hence the proper selection of strips that form a cluster is important. Random noise at the edges of a cluster can easily cause the precision to deteriorate.

The Eta method uses the data of only two strip to measure the cluster position: the strip with the largest signal in a cluster and its largest neighbor. The position is calculated as the weighed mean position of these two strips, weight being the signal of the strips in question. In the case of a one-strip cluster, the hit position is the strip position. If the actual charge sharing in a detector is small, the Eta method can outperform the CoG: the relevant positional information is coded into the two strips studied by the Eta algorithm. Channel thresholds can be lowered in a clusterizer, since the number of strips used for position estimation[4] and hence noise sensitivity does not increase.

[3]Events where spatial distance between two subsequent tracks is small compared to the track-induced cluster width must be handled separately.

[4]Widening of one-strip clusters to two-strip clusters excepted.

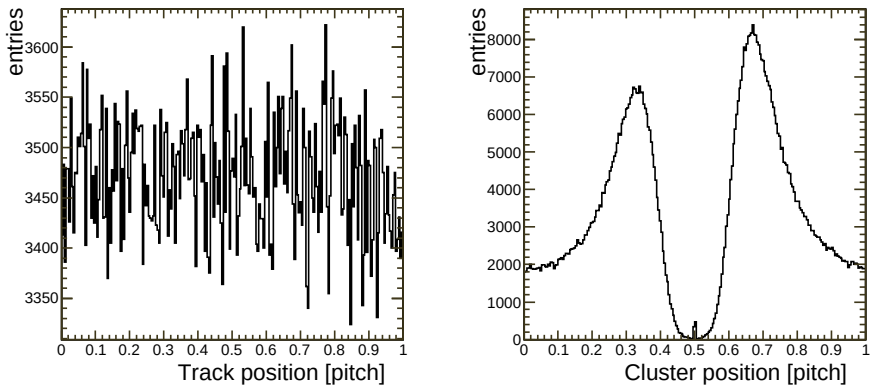

Figure 4.5: Positional distribution of clusters (right) and tracks projected to detector surface (left) in a unit cell plot. The strip position is at x $= 0.5$. This detector (Det. 1, see p. 33) does not have an intermediate strip.

The actual charge sharing between the two strips is not linear. Therefore, the reconstructed hit positions do not usually follow a flat distribution inside the unit cell (Fig. 4.5). This systematic error can be compensated using a calibrated version [59] of the hit point algorithm.

The first assumption behind the calibration is that the actual distribution of particles in a unit cell is constant. Considering the width and shape of the particle beam compared to the detector pitch, this is usually a good approximation (Fig. 4.5). The other assumption behind the calibration method is that the position reconstructed without calibration is a monotonously increasing function of the actual hit position within the unit cell. If these assumptions are correct, then a calibration function can be calculated in such a way that the reconstructed positional distribution of the reconstructed hit positions becomes flat. The calibration increases the noise sensitivity of the system: the second assumption listed above does not always hold good as a result of noise. The calibration may improve the resolution by correcting the non-linearities but could also worsen the measurement as a result of the increased noise sensitivity.

Track reconstruction

In track reconstruction, a track is formed out of the measured hit points. There are several possible algorithms, such as the Kalman filter [60] and Road search. In testbeam-like environments, an exhaustive search is also possible.

In the Kalman filter, first, a track candidate or several track candidates are constructed. Then the track candidate is propagated through the telescope, layer by layer, and the track properties are re-adjusted after each measurement. Once the construction is ready, the process is repeated in reverse order to smooth the candidate. Finally, the track candidate is accepted if it fits the measurement data well enough. Other acceptance criteria, such as the number of data points used in the fit, can also be applied.

Typically, the purpose of the reference system is to find high-quality tracks, and to reach the goal all the tracks that do not appear good are dropped. In SiBT07 data analysis, only those events where the track candidate contained a hit from all the reference detectors were used in the analysis of the device under test. The quality of the reference tracks was occasionally elevated by using additional cuts on the tracks. The use of untypically wide clusters in track reconstruction was occasionally prohibited, in order to minimize the probability that, e.g., δ rays would shift the barycenter of the cluster. A χ^2 cut is also used to filter out questionable tracks.

In track-induced clustering analysis it would, however, also be important to know which parts of the device under test were not hit by a beam particle. In this case, not only should failed

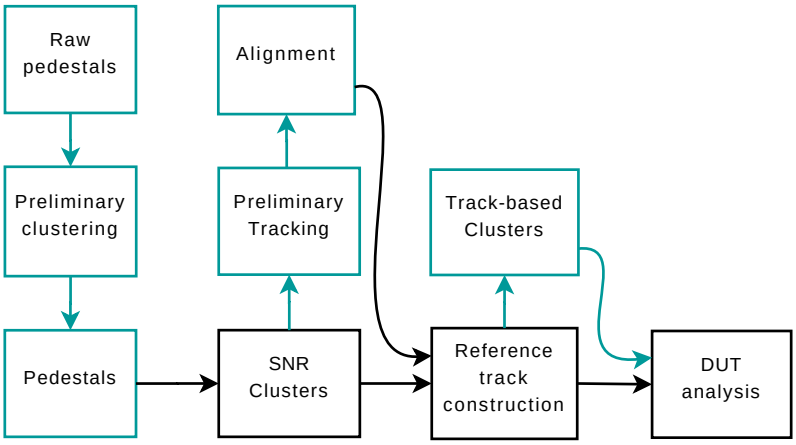

Figure 4.6: A simplified analysis flow. The mandatory steps are drawn in black, the optional steps in cyan. See text for details.

track candidates be dropped but the system should actively seek non-reconstructable tracks, too, and have a way of informing the user when the existence of a track in a certain area is unknown. In the testbeam environment, where events are simple, the most straightforward filter is where all the filtering takes place in event selection; the event is either fully usable or not usable at all.

Alignment

To reconstruct the reference track, one has to know the detector positions with an adequate precision. This can be achieved by, e.g., track-based alignment; position-sensitive detectors measure their own position by comparing the detector response to the reconstructed track. Hit and Impact Point (HIP) [61, 62] and Millepede [63] algorithms are used to align the CMS experiment; the alignment of SiBT and FinnCRack is done using the HIP algorithm.

In track-based alignment, the actual position and direction of the tracks is not known. Therefore the system needs to be constrained, e.g., by fixing the positions of some of the detectors [62]. If the system is overly constrained, the system does not align well. If the system is underconstrained, the alignment does not converge. Track-based alignment has its challenges: the detector physically has six degrees of freedom[5], but the strip detector measures the hit position in one[6] co-ordinate only. In test beam environments, where the variations in track directions are small, the alignment in the direction of the beam might not always be stable and could be sensitive to minor errors in the reconstruction.

Work flow

The analysis begins with a pedestal run. Initially, the pedestal values are not known, and hence it is not possible to use cluster exclusion code. To overcome this, "raw" pedestals are first calculated without cluster exclusion, and the pedestal calculation step is then repeated with cluster exclusion enabled (Fig. 4.6). The pedestals are marked as infrequent in Figure 4.6, since the same pedestal values can be used for a large number of runs if the operational conditions do not change.

Valid pedestals allow clustering and hit point assignment to be performed. Full tracking requires alignment to have been done. Alignment is computationally heavy compared to the

[5]Real detectors can also bend, experience thermal expansion, and so on. These small effects are ignored here.

[6]The strip have a finite length, which restricts the hit position in another co-ordinate. The detector spawns a plane in a geometrical way of speaking. The measurement takes place in that plane, which constrains the system, too.

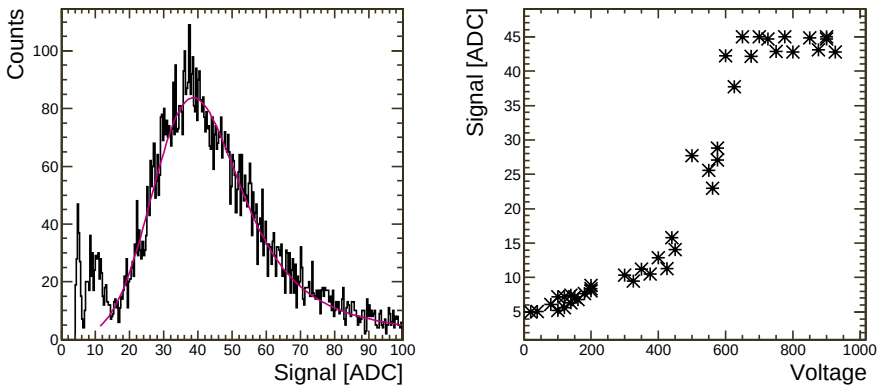

Figure 4.7: A signal height distribution (left) and a signal-versus-voltage graph (right). A convoluted Landau and Gaussian function fitted to the signal height distribution is also drawn. The data shown are from the barely working test Detector 6 (p. 33).

other steps, and it is typically done separately and the same alignment results are applied to a large set of runs as long as the system is not touched. In a testbeam-like environment, it is rather easy to accidentally touch the system in a way which makes the relative positions of the detectors change significantly. In the case of SiBT, e.g., changes in temperature count as touching the system. Track-based alignment requires tracking to be capable of being done. This is shown as "preliminary tracking" in Figure 4.6.

Figure 4.6 does not contain some of the steps discussed earlier: The hit point assignment is included into cluster construction. Similarly, noise calibration is included into pedestal calculation and common mode noise calculation everywhere where a re-iteration of data is needed, initial pedestal calculation excluded. One should notice that none of the mandatory boxes in Figure 4.6 contain noise calculation. Since noise is usually a key player in obtaining interesting results for the devices under test, some of the optional steps are optional only with quotation marks.

4.2 Analysis of the Device Under Test

The objective of a beam test is often to demonstrate that a device under test can be used to find the beam particles. Sometimes the objective of a beam test analysis is to obtain results which reflect the properties of the device under test as well as possible, and are affected by the characteristics of the measurement system as little as possible. The data analysis of a DUT differs somewhat depending on the goal of the measurement. The text below concentrates on the latter goal, but the former one is also addressed.

Event selection

Only a subset of the recorded events is used for analysis of the device under test. The inclusion of events where there is no reference track or the reference track does not penetrate the DUT into data the used to analyze DUT would make interpreting the results overly complicated.

It is beneficial to define the DUT properly. Let us assume that the properties of a detector material are being studied, and that *bonding*, i.e., connecting the detector to read-out has not been completely successful. The contribution of malbonded strips to the data should be masked out in the analysis to ensure that the results reflect the research question. However, if the detector properties caused the bonding to fail, the question of masking malbonded strips is no longer that straightforward. Similar choices can also be faced with strips that underperform other ways.

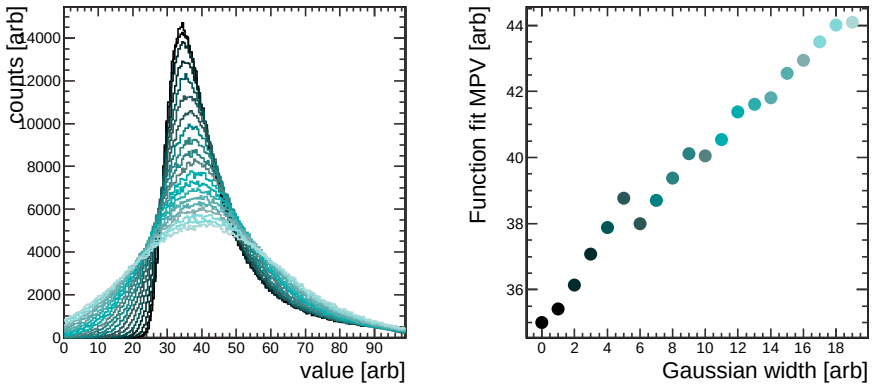

Figure 4.8: Landau distribution convoluted with various amounts of Gaussian noise (left). The plot on right-hand side shows the fitted most probable values (MPV) of the simulated data plotted in the histogram on the left-hand side.

The least-biasing way to address the problematic strips is to filter out both the measurement data of those strips and the reference data associated with those strips. In other words, the data of a masked-out strip should be removed in a way which prevents any contribution to noise, cluster, and common mode construction. In addition, all the events where based on reference track a masked-out strip would be expected to belong to a cluster should be masked out too, to avoid, e.g., the biased measurement of detector efficiency (see p. 28).

Signal

The signal is the response of the detector to a beam particle. The initial response of the detector to the beam approximately [64] follows the Landau distribution [65, 66]. When the charge is collected out of the detector, amplified, shaped, and otherwise modified as previously described, Gaussian noise is added to this data [67] in the analog readout chain.

The signal value of a cluster is often defined as the sum of the signals of all the strips of a cluster, after pedestal and common mode corrections. Sometimes the leading strip signal, or the sum of the signals from those strips used in hit point assignment, is also used as the cluster signal. The signal value of a cluster depends on the number of strips included in the cluster, and therefore it depends on the clustering algorithm and on the clustering thresholds used.

When the signal response of a detector is being determined, a histogram of the measured cluster signal values is produced. These histograms are often called Landau plots; see, e.g., Fig. 4.7. A convoluted Landau and Gaussian function (LG) is then fitted to the histogram [66]. The signal value of a run is the argument of the fit function for which the value is at its maximum. The amount of Gaussian noise affects the signal value acquired in this way (Fig. 4.8). This could cause a small systematic error to the signal values if the amount of noise in, e.g., the readout varies.

If clusters from some events have been omitted, which could easily happen if, e.g., none were found, the distribution no longer represents the true detector response to the particle (Fig. 4.7) but a typical response when the response is above an acceptance threshold. If the event selection described above is done properly, the existence of missing clusters should be included into the results. Track-induced clustering avoids this problem. In SNR-based clustering, missing clusters cannot be properly included into the cluster signal histogram prior to function fit and therefore they must be addressed differently.

The signal values are measured in ADC units. Eventually, one sometimes wants to convert the signal values to electrons. The conversion is straightforward if the response of the data acquisition is linear and the coefficient can be measured.

Usually the signal is calculated for track-associated clusters only. As a consistency check, it is also beneficial to calculate the signal of non-track-associated clusters. The assumption behind this check is that the signals of track-associated clusters originate from the particle being measured and the signals of non-track-associated clusters originate from noise tails. The distribution of non-track-associated signals should not follow the Landau statistics. If the shape of the signal distribution of non-track-associated clusters follows that of the track-associated clusters (see Figure 4.7) and especially if the MPV of the Landau corresponds to that of the track-associated clusters, the detector might not be responding to the beam at all.

Noise

The noise is calculated separately for each readout unit (p. 20), and comprises detector noise and readout noise. A noise of the readout front-end may depend on the input capacitance [44], and hence the straightforward use of unbonded channels to estimate the readout contribution to the measured noise can be biased.

Usually, the noise is assumed to follow the normal distribution. This assertion should, however, be verified before drawing conclusions about the noise values. Especially if the noise is not Gaussian (Fig. 4.9), then reporting efficiency (p. 28), specificity (p. 28), and the actual noise shape [67], in addition to the signal and the numeric value of the noise, are recommended.

The noise of an individual cluster is constructed of the noise values of the strips that belong to that cluster. In a simple cluster-finding algorithm, each strip must pass an SNR threshold to be included (p. 20). Assuming that the signal of the cluster is calculated as the sum of the strip signals, the cluster noise could simply be the sum of the noise values of the cluster strips. A cluster noise calculated in this way would be compatible with the cluster signal in the sense that a corresponding SNR value would reflect the average SNR of one strip in a cluster. This choice makes wide clusters appear more noisy than the narrower ones are. Therefore, increasing the clustering thresholds would appear to lower the cluster noise, which might not be what is wanted. An approach used by the CMS is to divide the sum of cluster strip noises by $\sqrt{N_{\mathrm{strips}}}$, to make the cluster noise values comparable with the strip noise [66]. This is also the noise definition of the SNR-based clustering results described here. One could also define the arithmetic mean or another mean of the strip noises to be the cluster noise.

The noise is a property of a strip. However, sometimes it would be convenient to present the noise of the whole detector as a single number. A common way to calculate the detector noise is to calculate a detector noise from the individual cluster noises described above. It would also be possible to calculate the detector noise from the individual strip noises. The conceptual difference is that in a cluster noise-based approach the strips are weighted with the beam profile. In other words, the higher the probability that a strip was part of a cluster accepted to the analysis, the higher the weight of that strip in the calculated detector noise. This is good in the sense that if the noise is compared to signal, then all the strips have contributed to both numbers with a similar weight. When a non-clustering approach to data analysis is being used, the noise could also be calculated as the standard deviation of the control measurement described on page 22.

Since there are several ways to calculate the detector noise, one should report the method used to calculate noise in order to avoid the accidental comparison of incompatible numbers later.

Signal over Noise Ratio

The commonly-used signal-over-noise ratio allows the comparison of detector goodnesses from setup to setup. If one can assume that the signal and noise levels are homogeneous in space and that the noise is Gaussian distributed and the shape of the signal distribution is also known, the SNR directly gives an impression of the goodness of the acquired data and the frequency of fake clusters.

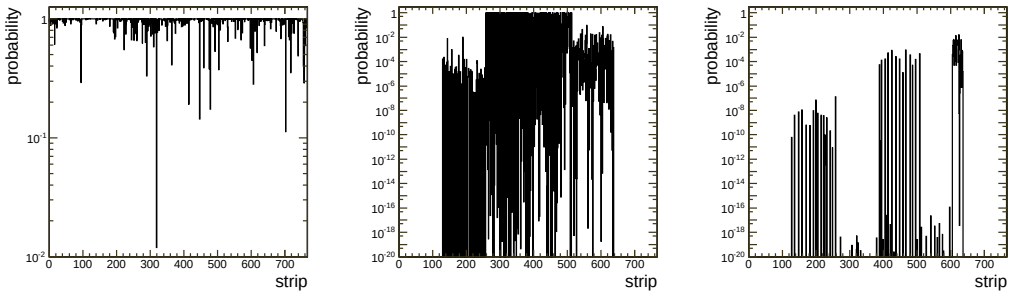

Figure 4.9: The Gaussian-ness of noise using the Kolmogorov-Smirnov test, calculated separately for each strip. Values near one indicate that the common-mode subtracted strip noise follows the Gaussian distribution. Detector 0 (see p. 33), shown on the left, has not been irradiated and works well; Detector 12, in the middle, is an irradiated one, and is considered to work. Detector 6, shown on the right, is not working properly (Fig. 4.7).

Signal-over-noise values can be calculated in a number of ways: first, there are many ways to calculate the signal and many ways to calculate the noise. In addition, a SNR can be calculated separately for each cluster and then generalized to the SNR of the detector, or one could first generalize the signal value of a run and the noise value of a run and then carry out the division. These methods produce somewhat different numerical SNR values.

Efficiency and Specificity

Efficiency is the probability of the detector recording the signal of the incoming particle. It is defined as the probability that there exists a track associated cluster in the detector for a reference track, where track-association is defined by a residual cut and the clusters are defined by the clusterization algorithm (p. 20). The measured efficiency depends on the residual cuts and clustering thresholds used (Fig. 4.10). Typically, the efficiency of a working detector should be above 99%.

In track-based clustering (p. 21), efficiency and specificity cannot be measured, since all the tracks have an associated cluster and all the clusters are associated with the reference track by definition.

The efficiency depends on the parameters of the clustering algorithm. It would be possible to tune the thresholds close to zero in a way which would produce reasonably high efficiencies for a non-working detector at the cost of the detector being full of fake clusters, i.e., clusters that originate from noise instead of the particles being measured. A way to overcome this problem is to quote the positive predictive value (also called specificity and purity) of the clusters that are found, the probability that a cluster that has been found is track-associated. Lowering the clustering thresholds to an artificially low level increases the numerical value of the efficiency (Fig. 4.10). However, it lowers the specificity and therefore the combination of these two numbers is a superior estimate of the particle-finding capability of the detector compared to the use of the efficiency only.

If a detector noise is Gaussian, a reasonably high signal-to-noise threshold ensures that there are relatively few noise clusters, and therefore traditionally there has been no need to quote the specificity. However, if the actual noise distribution is not Gaussian, then this assertion does not hold good, and the specificity plot would serve as a warning sign in data analysis. Specificity is not a standard performance number in the sense that it is usually not reported. The definition of specificity quoted above has the problem that it is sensitive to the number of read-out channels in a detector.

It would be convenient to have a single performance number that characterizes the particle-finding capability of a detector. A super-efficiency would be useful, especially when plotting the

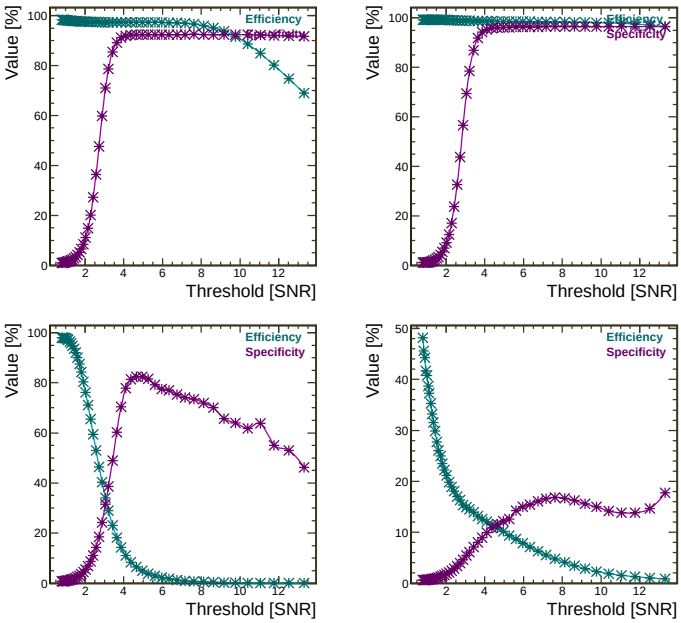

Figure 4.10: Efficiency and specificity depend on the clustering thresholds. These example plots demonstrate that the choice of thresholds does affect the results. Data from Detectors 0, 1, 4, and 10 are shown.

particle-finding capability of a detector versus its operating conditions. One possible candidate is the multiplication product of the efficiency and specificity numbers. Defined this way, super-efficiency would have the following characteristics: 1) for a good detector the number would approach one; 2) for a non-working detector the number would be close to zero; 3) sensible clustering parameters produce high values of super-efficiency. I would not, however, promote the usage of super-efficiency defined this way, since efficiency and specificity are not symmetric; a detector that finds particles with an efficiency of 90% and produces no noise clusters is worse in many uses than a detector that finds all the particles and in addition produces one false cluster for each nine correctly reconstructed ones. Super-efficiency defined in this way would be the same in both cases.

Residual and Detector Resolution

The residual of a cluster is the positional difference of the reconstructed cluster position and the reference track impact point projected onto the detector surface. The residual distribution is the distribution of cluster residuals.

The residual of a run is the standard deviation of the residual distribution. Usually, a residual cut is applied before calculating this residual. The use of a residual cut can be justified by arguing that this limits the data to track-associated clusters only, and that random clusters far away from the track center would have a large impact on the calculated residual. While the argument is correct, there is a potential problem associated with this approach: when only clusters close to the track position, in other words, those clusters that provide evidence of a small residual, are allowed to contribute to the measurement results, falsely good-looking results can be obtained. The problem associated with the choice of a residual cut is diminished if the same residual cut is also used when calculating the efficiency (and specificity) numbers for that detector and publishing them together. A narrow residual cut, which makes the residual appear “good”, lowers the other two performance numbers.

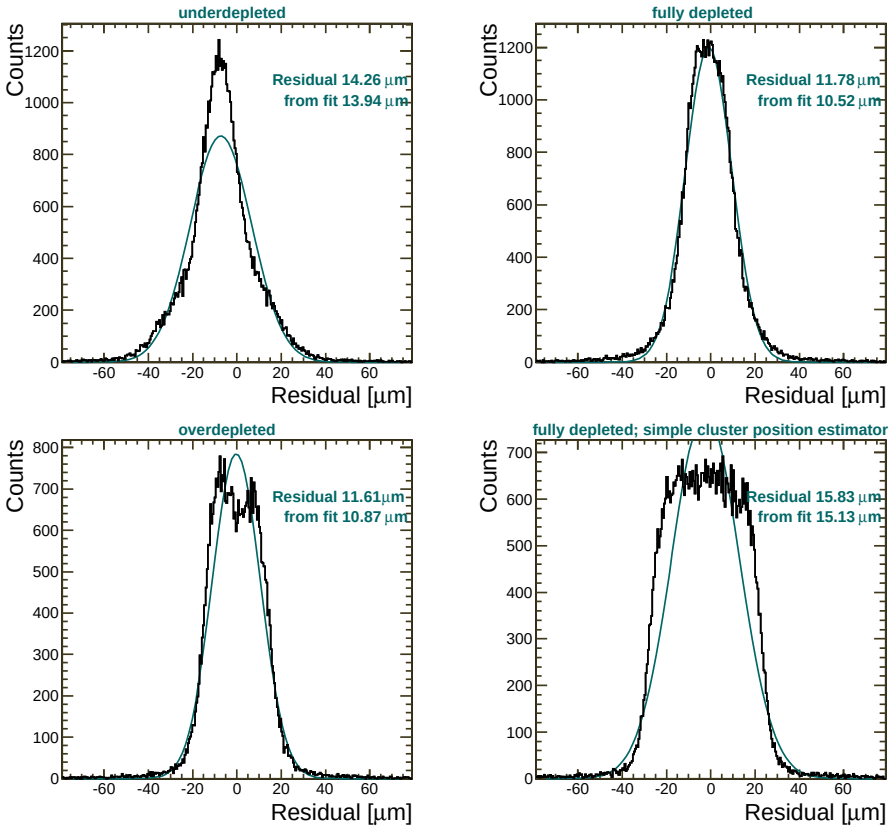

Figure 4.11: Residual distributions. In these plots a residual cut of 50 μm was used to select the clusters included in the calculation. All the plots show the response of detector 1 (p. 33); the detector bias voltage and the choice of the cluster position estimator algorithm varies.

A more common used approach is to fit a Gaussian distribution to the data, and to use the function instead of the distribution to calculate the residual. The benefit of this approach is that it is rather insensitive to the residual cut. There is no guarantee that a residual distribution would actually be Gaussian distributed, though [40, 68]. Usually, this method works sufficiently well and can be used to estimate the residual of the detector (Fig. 4.11). Sometimes the FWHM of the residual distribution has been used [69], although that approach appears to be uncommon in position-sensitive data analysis.

The resolution is the residual of that detector, where the contribution of the track uncertainty has been corrected. If the track position and cluster positions are independent (correlation via beam particle excepted), the detector resolution can be calculated as a quadratic difference of the residual and the error of the impact point of the track, $\sigma_m = (\sigma_r^2 - \sigma_f^2)^{1/2}$.

The resolution of the detector can be expressed as a single number if all the clusters in that detector are equally precise.

4.3 Summary of the analysis procedure

The aim of the analysis is to obtain the desired properties of the device under test. An easy way to approach this is to discard all data that could lead to biased results as a result of the measurement system. Typical examples are discarding data measured at times when the temperature or

humidity would not have been stable or discarding data from events where the reconstructed reference is bad or it is not certain that all the reference tracks in the event have actually been properly reconstructed.

There are two targets in a beam test analysis:

- to characterize the detector properties
- to demonstrate the detector's capability to act as a position sensitive detector.

The analysis must match the set goal. If detector properties are being studied, the SNR thresholds should be as low as possible, or clustering should be abandoned altogether. Track-induced clustering has several advantages over SNR-based clustering in the study of detector properties and has smaller chances of producing biased results.

If detector operation is being demonstrated, SNR based clustering with a higher SNR cut level should be used, to keep the specificity at a reasonable level; abundance of non-particle induced clusters complicate track reconstruction. Studying efficiency together with specificity reveals the problem in data associated with a wrong clustering threshold choice.

Data often need to be filtered. It is important to use the same filter to extract all the performance numbers. Optimizing the cuts separately for each performance number might lead to a wrong impression of the true performance of the device being characterized. This can happen accidentally if the "cuts" are made when plotting data. Falsely good-looking results can also be obtained if the data are skimmed in a way which hides real defects in the device under test.

Chapter 5

Measurements

As of summer 2010, four distinct measurement periods have been carried out using the SiBT07 apparatus. Test runs where only the operation of the SiBT apparatus itself was studied are not included in that number.

The SiBT07 tests took place at the CERN H2 test beam area in Prévessin, France. Most of the details in the following description are from the summer 2008 test run. Article [**VI**] concentrates on describing the results of that particular test run, while article [**VIII**] contains a summary of the results of all the runs. Summer 2008 is a typical SiBT beam period, and its flow of actions is communicated below. The beam test periods of SiBT99 were also similar.

Similar measurements done using FinnCRack progress slowly compared to the beam tests, because of the slow data acquisition rate. Like the beam telescopes, FinnCRack also requires continuous supervision and regular maintenance. When the apparatus is switched on, the operators need to be present and are frequently interrupted by the FinnCRack monitor. As the data-acquisition can continue for weeks, this work-load introduces a price tag in man-hours to the data acquired, and hence sets an upper limit to the amount of testing that can be done despite the continuous availability of cosmic particles. It might be possible to reduce the workload caused by the apparatus and thus overcome this limitation in the future. Regardless of the work-load aspects, the need to have results ready by a pre-determined day limits the amount of data that can be acquired using the cosmic setup.

5.1 SiBT 2008 beam period

The SiBT was installed in the beam area in July 8th, 2008 and disassembled almost 15 days later, on July 23rd.

Overall, the tests proceeded smoothly and successfully. The SiBT had been upgraded in many ways since the previous test. The maximum trigger rate was increased from its previous value of 23 Hz to approximately 130 Hz. A previously unused slot of the Vienna box was successfully put into use, allowing two DUT's to be measured at the same time inside the box. The external Coldfinger box was added to the measurement system. There was a novel temperature control, monitoring, and logging applet and a detector bias voltage applet. Additionally, a larger amount of condition data compared to previous tests was being automatically logged.

There were some obstacles during the data-taking period: two components, upgraded since the previous test, were found to be mechanically incompatible; a critical part of the control ring was destroyed during set-up by electrostatic discharge; a replacement control ring was found to be incompatible with the rest of the setup; first attempt to fix the critical part failed; the readout

power distribution became unstable; a readout computer 'died' as a result of a broken motherboard capacitor; the upgrade in SiBT trigger rate caused a data-acquisition computer to become unstable; an amplifier in one of the readout chains stopped working; the XY table that the setup was located on partially stopped working, making it difficult to re-insert the setup into the beam after it had been lowered for repairs or module exchange, and the limited availability of experts. In addition to these, the SPS accelerator that provides the H2 beam had serious problems during that time. The total SPS beam-off time during the test period was almost ten days.

5.2 SiBT 2008 measurements

Six of our DUTs were measured during the 2008 beam period: four magnetic Czochralski detectors irradiated to various fluences and two float zone silicon detectors, one of which was not irradiated. Two detectors belonging to another research program were measured during that time, too [71].

Detector 10 (Table 5.1), which had the highest irradiation fluence, was measured in the Coldfinger box, while the others were placed into the Vienna box.

The limited amount of data acquisition time available caused a few minor alterations to the research plan; the runs of some detectors were shorter than originally planned, and only two voltage scans were done on each device under test.

The temperature inside the Vienna box was too high to allow Detector 8 to be fully biased; the leakage current was high enough for the device to experience a thermal runaway. Biasing Detector 10 to the target voltage succeeded, as it was possible to cool this detector to colder temperatures and the thermal connection to the heat sink was better in the Coldfinger box compared to the case in the Vienna box. The measurements of Detector 10 were, however, harmed by cross-talk between a data acquisition-related ethernet cable and the cable delivering the analog measurement data away from the Coldfinger box (p. 15). This flaw was unfortunately not discovered online, and caused the noise analysis of this detector to be challenging.

The verdict is that the data of four detectors are of high quality, and the two mentioned above are usable with remarks. Despite the short runs, no data points needed to be discarded because of insufficient statistics.

The analysis of the 2008 beamtest results published in [**VI**] was performed in the manner

Table 5.1: List of detectors discussed in this introductory part of the present study.

Detector	Type	Source	Fluence	Published
0	nFZ	HPK	0	[**III**] & [70]
1	nFZ	HIP	0	[**VI**]
2	nMCz	HIP	0	[**VIII**]
3	nFZ	HIP	1.0e14	[**VIII**]
4	nFZ	HIP	2.2e14	[**VI**]
5	nMCz	HIP	6.1e14	[**VI**]
6	nMCz	HIP	1.0e15	N.R.
7	nMCz	HIP	1.1e15	[**VI**]
8	nMCz	HIP	1.6e15	[**VI**]
9	pMCz	HIP	2.0e15	[**VIII**]
10	nMCz	HIP	2.8e15	[**VI**]
11	nMCz	HIP	2.8e15	[**VIII**]
12	nMCz	HIP	4.9e15	[**VIII**]

HPK denotes a detector made by Hamamatsu Photonics K.K., HIP a detector made at the Helsinki Institute of Physics

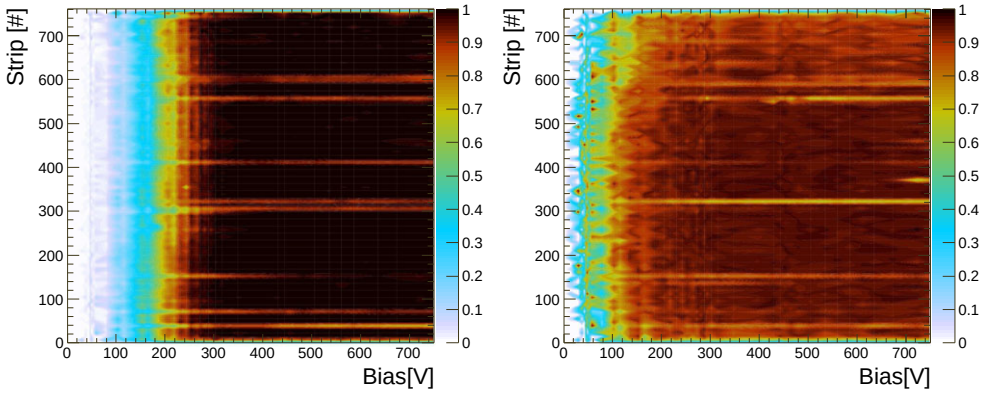

Figure 5.1: Efficiency (left) and specificity (right) of Detector 4, plotted separately for groups of eight strips. A clustering method with the cluster acceptance threshold of 4.0 was used to generate this plot.

described earlier in this thesis. A low signal-over-noise threshold was used in the cluster construction, to reduce the risk of biased results such as those illustrated in Figure 6.2 and also in the following chapter. Track-induced clustering was considered an experimental method at the time this analysis was done and therefore only traditional clustering results were published.

5.3 Discussion

The devices under test performed as expected in the beam test, supporting the hypothesis that Magnetic Czochralski silicon would be a suitable detector material for S-LHC use. The other beam tests and analyses produced similar results. The detectors showed anomalies, e.g., low-efficiency regions. These can all be explained by known errors in the DUT preparation.

The largest number of post-article discussions were on the resolution behavior of the irradiated float zone detector (Det. 4 in Table 5.1). The data of this detector were thoroughly checked and found to be correct. One possible trigger for those discussions was that the efficiency plot of that particular detector was not present in Article [**VI**]. Those data, originally left out because of a page limit and other reasons, are now visible in Figure 5.1. The efficiency of Detector 4 versus bias voltage behaves as expected: the efficiency is close to 100% when the detector is fully depleted. A few of the strips show a poorer performance (Fig. 5.1).

A similar resolution-versus-bias voltage behavior can be seen in the other float zone detector (Det. 1 in Table 5.1), too. Apparently, the resolution deteriorates towards the digital resolution in the over-biased case since charge-sharing between strips, and therefore the possibilities of interpolating the hit position diminish when the charge is collected more rapidly, despite the fact that the total collected charge continues to increase. The resolution also worsens in the underdepleted case, since the signal level approaches the SNR cut, making all the clusters one strip wide. The residual distributions in Figure 4.11 (p. 30) demonstrate this. This particular detector (Det. 4) has experienced a type inversion (p. 6). In the underdepleted situation the holes drift through a low or zero field on the way to the strips, which widens the charge cloud and makes the above problem worse. In the barely depleted case, only a few events have clusters. In this case the probability of the detector finding a cluster depends on the track distance from the closest strip. In the analysis that appears as an improvement in resolution.

Chapter 6

Results

The results of this work can be divided into two parts; results involving the measurement apparatuses and results acquired using the apparatuses.

6.1 The Telescopes

All three reference devices are able to measure particle tracks. The parameters listed in Table 6.1 are values obtained during device use. The trigger rate, low-temperature operation, and stability of the devices could be further improved if there was enough need to justify the amount of work needed to carry out those upgrades. The quality of the reference tracks is good enough to allow the devices to be used as reference devices in the expected way.

SiBT99 is a rather space-efficient (p. 14) apparatus and its assembly is rather fast, assuming that all of the components are properly functional. In contrast, the building blocks of SiBT07 and FinnCRack are meant for other uses and working with the setups is time-consuming; so far the assembly of SiBT07 has always taken more than one full day. The number of cables and other supporting equipment (Fig. 6.1) in the vicinity of the detectors illustrates the problem. One poorly routed electrical wire is sufficient to ruin the measurement. The assembly of FinnCRack

Table 6.1: Comparison of the telescopes. Trigger rates are shown as averages over an entire run. They depend on, e.g., the SPS spill structure for the beam telescopes and are therefore approximate. The second low-temperature limit in case of SiBT07 refers to the additional container (p. 15). Generally, the values reported here differ from those in the articles because of improvements made to the systems since the articles were written.

Feature		SiBT99	SiBT07	FinnCRack
trigger rate	[Hz]	200	100	3
Reference track resolution	[μm]	3.5	4.0	19
Track efficiency	$\frac{\text{tracks}}{100 \text{ triggers}}$	90	65	6
Signal-to-noise ratio		29	29	35
DUT slots	#	1	3	6
Reference area	cm^2	5.6×5.6	3.8×3.8	108×9.2
Low temperature limit	[°C]	N/A	-25/-53	-20
Synchronization to external devices		easy	complicated	not done

The reference area of FinnCRack is not exactly square-shaped, and therefore the above table slightly overestimates the usable reference area. The actual reference area of all the telescopes is reduced if the reference detectors are not inserted into their nominal positions.

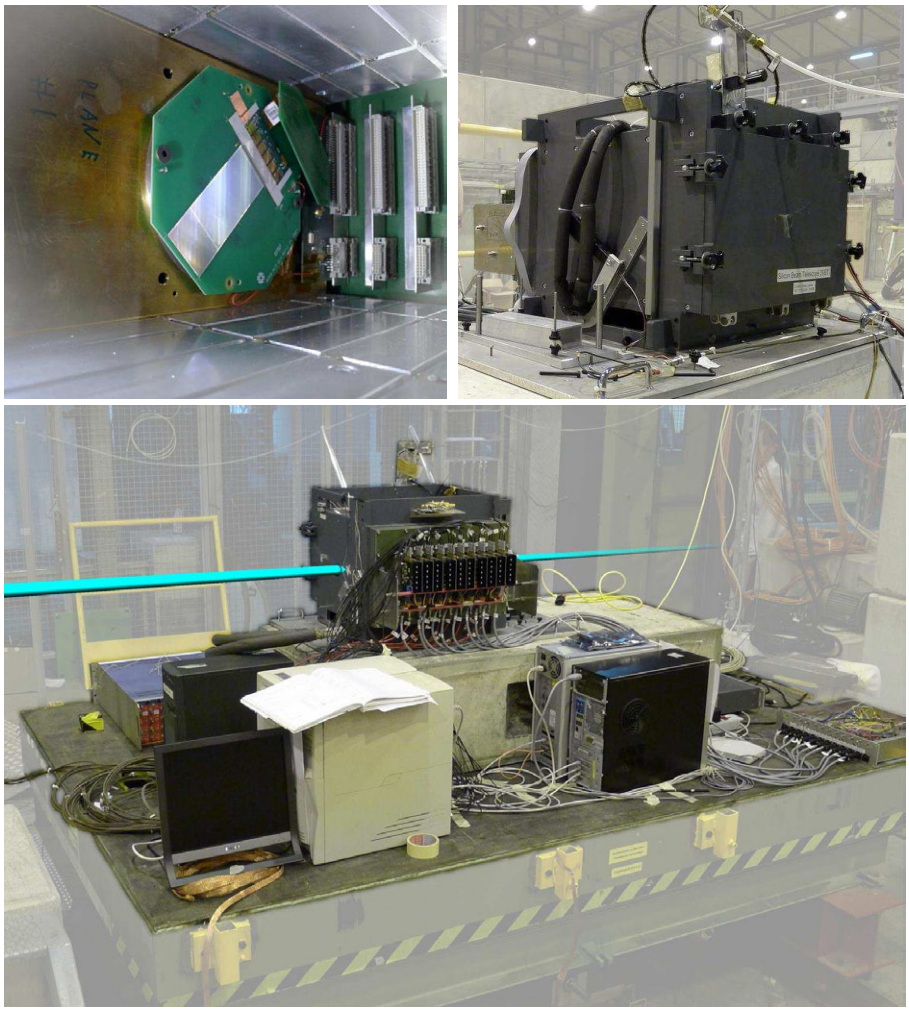

Figure 6.1: The SiBT07 apparatus: Detectors are assembled on octagon-shaped modules (top left), which are insterted to the Vienna box (top right). A photograph of the assembled setup is also shown in the lower part of this figure. The position of the particle beam is shown in cyan color in the lowermost picture. These photographs have been post-processed for clarity.

is even more slow, albeit straightforward, thanks to the assembly procedure being documented. There is more tacit knowledge associated with the SiBT07 setup.

SiBT99 does online data reduction with hardware. This approach has its benefits, but it induces the risk of permanently losing data. FinnCRack is able to work with and without online data reduction, while SiBT07 always stores all the data. Considering the nature of these devices, the benefits of storing all the measurement data outweigh the associated drawbacks. On the basis of the experience acquired using these devices, the best system would be one where all the data of all the devices under test were stored. To minimize problems associated with huge data files, the data of the reference detectors could be clusterized online in the majority of the runs.

These apparatuses are complex; they are made by a small team and they are unique[1] pieces of hardware. Although they can produce proper data, infrequently appearing unresolved problems remain in all these devices. This is unsurprising, considering the complexity and the amount of testing done on the final systems. The direct consequence is that the devices need to be constantly

[1]There is another cosmic rack [45] similar to FinnCRack at CERN.

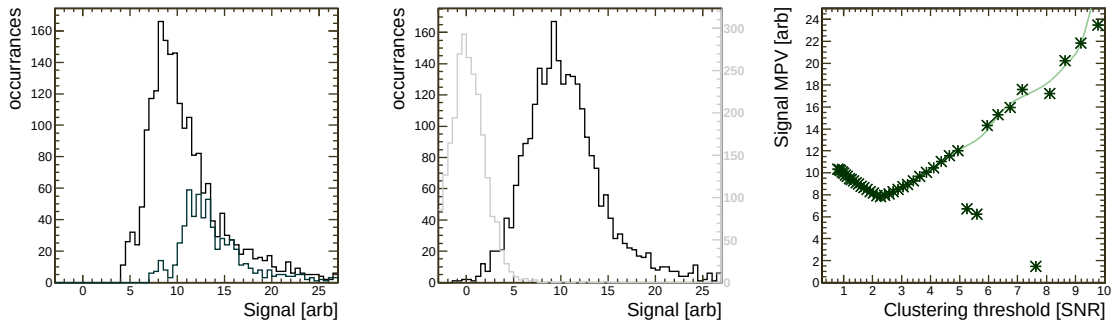

Figure 6.2: Landau plots of Detector 3 (being underdepleted) data acquired using SNR cut thresholds of 3 and 5 (left) and using track-induced clustering (center). Signal value (p. 26) dependence of clustering threshold (right). The same data were used to obtain all the curves. The control plot (p. 22) of the track-induced clustering is also shown in the centermost plot.

monitored during data taking, to ensure the satisfactory outcome of the tests. In addition to onsite shifters, offline data analyzers that can concentrate on the peculiarities of the data that are collected and therefore have better odds of spotting the less obvious hardware problems during beam time are also needed. This situation is unlikely to change, as discussions about re-building SiBT07 have already begun.

The FinnCRack project also had other goals, in addition to reference track production, such as usability as a CMS software development platform during CMS construction. These goals were eventually not met.

The data analysis of the devices has been described in the earlier chapters. The analysis of devices under test has repeatedly demonstrated that all the performance parameters listed here need to be studied before any conclusions are drawn. Two examples demonstrating the importance of complete analysis, also in cases where only a subset of the results is interesting for the particular research question, are described below.

- Figure 4.2 illustrates one example event with a large number of noise-induced clusters. The signal-to-noise ratio and efficiency data appear to be what is expected. Omitting the study of specificity and noise cluster signal distribution when such events appear frequently might lead to a false impression of actual detector performances.
- The voltage scan results of Detector 6 (Table 5.1, p. 33) illustrated in Figure 4.7 show a large signal value for large detector bias values. A more detailed analysis shows a different picture. There is no difference between the clusters associated with tracks and other clusters. In addition, the existence of a track increases the probability of the formation of a cluster only slightly. The increase in the "signal" with voltage is caused by an increase in noise. The signal distribution happens to look Landau-like, as demonstrated by the function fit. Clustering is done in signal-to-noise values, but the signal is plotted. Since the noise is not uniform in space, the shape of the noise tail can imitate the Landau distribution and be misinterpreted as a real signal. The fact that there are enough clusters to cause the statistics of the signal plot to be at the expected levels is due to the fact that the noise is, in addition to being non-uniform in space, also not Gaussian distributed in time. A careful analysis reveals that Detector 6 does not work at, all despite the promising preliminary results.

It is generally known that if a decently high SNR cut is applied to the data, then only a few noise-induced clusters remain in it. The above is true if the noise is correctly calculated and the noise follows the Gaussian distribution. Those assumptions might, however, not always be true (Fig. 4.9). Noise performance reporting in studies of radiation hardness is sometimes incomplete

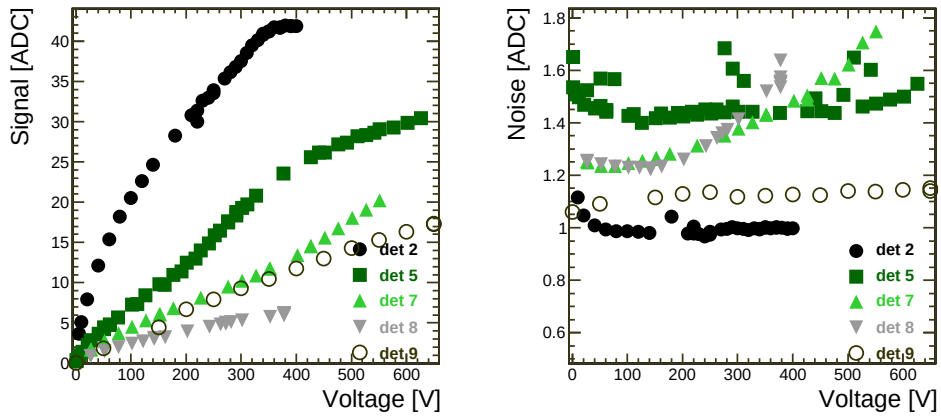

Figure 6.3: Signal (left) and noise (right) versus detector bias graphs. Detector 9 (p. 33) was measured at a significantly lower temperature compared to the other ones, which might have affected the noise behavior.

in the sense that the Gaussian-ness of the noise is not mentioned. On the basis of the limited results of this study, noise being Gaussian should not be taken for granted.

In a low-SNR condition, the choice of clustering threshold may affect the measured signal values: a high cut value causes the lower end of the actual cluster distribution to be discarded, which results in the signal value appearing higher than it actually is. If the threshold is artificially low, then the inclusion of noise may make the signal value appear higher than it actually is. This behavior is illustrated in Figure 6.2, where detector 3 is biased with a mere fifty volts to emphasize the artifact. If the clustering threshold is kept constant, then this can induce a systematic false increase into the measured values. This possible bias in the measurement results can be avoided by using track-induced clustering (TIC) instead of SNR-based clustering when charge collection efficiency is of interest. Some biases in noise and common mode calculation can also be avoided by the use of the TIC method.

There are many ways to calculate the key performance numbers, such as the signal, noise, and SNR of a silicon strip detector, which produce slightly different numerical values. This should be taken into account when comparing measurement results against other results.

Traditionally there has been a clear separation between signal and noise in the silicon detectors, and questions regarding signal and noise have been straightforward to solve. When large surface areas need to be covered, the increase can be achieved at the expense of a reduced signal over noise ratio. When signals must be discriminated on the basis of their timings using multiple samples, the price tag is a reduced SNR. The same happens when detectors are operated for long periods in hostile environments that induce radiation damage in them. Therefore, understanding the operation of detectors in low-SNR situations is important and will become even more so in the future.

6.2 Radiation hardness of Magnetic Czochralski detectors.

Several strip detectors were measured in the test beam and their performance was characterized. Most detectors are magnetic Czochralski strip detectors and differ in their irradiation levels. A few float-zone silicon detectors were also measured. Most detectors were irradiated with protons, and some with a mixture of protons and neutrons. Both n-type and p-type detectors (p. 5) were measured, most detectors being n-type. Some detectors were measured with both forward and reverse biasing, but most were measured using the standard reverse bias setup only. The

detectors were measured at temperatures around -20 °C, though it was not always possible to reach that temperature because of problems in the cooling system. When forward biasing was being used, the temperatures were lower, down to -53 °C. These measurements are discussed in Articles [**VI**] and [**VIII**].

The results comprise the signal, the noise, the SNR, the charge-collecting efficiency (CCE), resolution, and the efficiency of the detectors (p. 26–29). The CCEs were calculated by comparing the measured signals to those produced by the unirradiated detectors. Sometimes the unirradiated detector used in this comparison was measured using a different beam test period and at a somewhat different temperature. The variations in temperatures may have affected the results slightly; reference detector data indicate that the systematic errors as a result of this are likely to be below 5%.

One important goal of the measurements is to study the feasibility of the detectors in future HEP experiments. This means that the detector performance is particularly interesting in the conditions in which the detectors of future HEP experiments will be operated. It is likely that the U_{bias} of the detectors will be limited to 600 V in a future upgrade of the CMS experiment.

The full depletion voltage of a detector depends on the irradiation dose [72]. The full depletion of the test detectors was typically above 600 V. Therefore it was not always feasible to measure the behavior versus voltage up to full depletion. Sometimes even the target voltage of 600 V was not reached because of the thermal runaway [32] effect.

The results indicate that increasing fluence reduces the charge-collecting efficiency, as expected. Magnetic Czochralski appears to be a good candidate as a detector material; the detectors can be fully depleted at 600 V until the dose of 6×10^{14} $\mathrm{n_{eq}/c}m^2$ (Det. 5 in Fig. 6.3) and have a CCE of above 50% and a signal-to-noise ratio exceeding ten at least up to the dose of 1.1×10^{15} $\mathrm{n_{eq}/c}m^2$ (Det. 7 in Fig. 6.3). The so-called p-type detector, which collects electrons instead of holes, shows some advantages over the standard n-type detector and should have similar characteristics at the dose of 2×10^{15} $\mathrm{n_{eq}/c}m^2$ (Det. 9 in Fig. 6.3). Operating the detectors in forward bias mode has some additional benefits over the reverse bias operation, and detectors irradiated to the dose of 5×10^{15} $\mathrm{n_{eq}/c}m^2$ (Det. 12) still produce a reasonable signal when operated in this manner. The downside of using p-type detectors rather than n-type detectors lies in module production being more difficult [73, 25]; the downside of forward-biased detectors lies in the fact that they need to be operated at lower temperatures, -53 °C in this case, which causes the cooling system of the experiment to be complicated.

Chapter 7

Summary

This thesis studies silicon strip detectors and the methods and equipment used to characterize such detectors. Three measurement apparatuses are presented: two versions of the Silicon Beam telescope and a cosmic rack. Hardware-wise, the two beam telescopes are rather different. The benefits of both approaches are discussed.

Both beam telescopes have been successfully used to study novel detectors. The cosmic rack is also capable of finding particle tracks and could also be used as a test bench in detector studies. Because of the success of past beam tests FinnCRack was oriented to different goals. All these apparatuses are unique instruments and are constantly being modified because of the changing needs of the research motivating these telescopes. Examples of research benefiting from the data of these devices are described in [74, 11, 12, 13, 71, 15, 16, 75]. The beam telescopes have, overall, been success stories. FinnCRack did not fulfill all of its objectives as a result of being late.

Silicon strip detectors have been used as position sensitive detectors in a number of applications. This thesis studies the characterization of such detectors nearing the end of their operational life. Careful analysis of such detectors has revealed opportunities to improve the data analysis itself. The data analysis of the silicon strip detector data typically follows the path described in earlier chapters. The set of results that are typically reported — charge collection, signal-to-noise ratio and efficiency — describe the performance of a detector well when the detector is working well. When the detector is not working well, these performance numbers do not always reveal it. This causes a risk of misinterpreting the true detector performance. The use of track-induced clustering and complementing efficiency with specificity lessens the likelihood of biased results.

Several Magnetic Czochralski silicon strip detectors were irradiated, up to the fluence of 4.9×10^{15} 1 MeV neutron equivalents per square centimeter. The post-irradiation performance was then measured using the above-mentioned telescope. The beam test results indicate that the n-type MCz-Si strip detectors can be operated with an acceptable SNR throughout the integrated S-LHC fluence in the strip layers of the future CMS upgrade. Overall, the study on the feasibility of Magnetic Czochralski detectors has been a great success.

The quality of the signal acquired can be elevated by using p-type sensors instead of the standard n-type sensors, or by using forward biasing of the detectors instead of the standard reverse bias. However, the engineering-related challenges present in these alternatives might render the n-type reverse biased MCz detectors to most favorable solution.

References

[1] Lyndon Evans and Philip Bryant. LHC Machine. *J. Instrum.*, 3:S08001, 2008.

[2] H.-A. Gustafsson et al. The ALICE experiment at the CERN LHC. *J. Instrum.*, 3:S08002, 2008.

[3] CMS Outreach material. `http://cms.web.cern.ch/cms/index.html` .

[4] S. Chatrchyan et al. The CMS experiment at the CERN LHC. *J. Instrum.*, 3:S08004, 2008.

[5] A. Tricomi. SLHC: The LHC luminosity upgrade. *Nucl. Instr. and Meth. A*, 596:43–47, 2008.

[6] F. Gianotti, M. L. Mangano, T. Virdee, et al. Physics potential and experimental challenges of the LHC luminosity upgrade. *Eur. Phys. C*, 39(3):293–333, 2005.

[7] I. Dawson. The SLHC prospects at ATLAS and CMS. *J. Phys.: Conf. Ser.*, 110(9):092008, 2008.

[8] CMS Collaboration. *Physics Technical Design Report*, volume I. CERN-LHCC-2006-001.

[9] R. Bainbridge et al. Production testing and quality assurance of CMS silicon microstrip tracker readout chips. *CMS NOTE*, 2004/016.

[10] M. Raymond and G. Hall. CMS microstrip tracker readout at the SLHC. In *Proceedings of the Topical Workshop on Electronics for Particle Physics*, Naxos, Greece, September 15-19, 2008.

[11] E. Tuominen et al. Test beam results of a large area strip detector made on high resistivity Czochralski silicon. *Nuclear Physics B (Proc. Suppl.)*, 125:175–178, 2003.

[12] P. Luukka et al. Test beam results of a proton irradiated Czochralski silicon strip detector. *Nucl. Instr. and Meth. A*, 568:72–77, 2006.

[13] P. Luukka et al. TCT and test beam results of irradiated magnetic Czochralski silicon (MCz-Si) detectors. *Nucl. Instr. and Meth. A*, 604:254–257, 2009.

[14] E. Tuominen et al. Recent progress in CERN RD39: Radiation hard cryogenic silicon detectors for applications in LHC experiments and their future upgrades. *IEEE Trans. Nucl. Sci.*, 56:2119–2123, 2009.

[15] J. Härkönen et al. Test beam results of a heavily irradiated Current Injected Detector (CID). *Nucl. Instr. and Meth. A*, 612:488–492, 2010.

[16] E. Tuovinen et al. Magnetic Czochralski silicon strip detectors for Super-LHC experiments. *Nucl. Instr. and Meth. A*, 2010.

[17] V. Tikhonov and R. Veenhof. GEM simulation methods development. *Nucl. Instr. and Meth. A*, 478:452–459, 2002.

[18] M. Mathes et al. Characterization of a Single Crystal Diamond Pixel Detector in a High Energy Particle Beam. *J. Instrum.*, 3:P12002, 2008.

[19] G. Ruggiero et al. Planar Edgeless Silicon Detectors for the TOTEM Experiment. *IEEE Trans. Nucl. Sci.*, 52(5):1899–1902, 2005.

[20] P. Holl et al. A double-sided silicon strip detector with capacitive readout and a new method of integrated bias coupling. *IEEE Trans. Nucl. Sci.*, 36:251–255, 1989.

[21] M. Bregant et al. The ALICE vertex detector: Focus on the micro-strip layers. *Nucl. Instr. and Meth. A*, 569:29–32, 2006.

[22] A. Zoboli et al. Initial results from 3D-DDTC detectors on p-type substrates. *Nucl. Instr. and Meth. A*, 612(3):521–524, 2010.

[23] M. Krammer. The silicon sensors for the Inner Tracker of the Compact Muon Solenoid experiment. *Nucl. Instr. and Meth. A*, pages 238–245, 2004.

[24] M. Huhtinen et al. Single-sided stereo angle silicon strip detector. In *Conference Record of the Nuclear Science Symposium and Medical Imaging Conference*, pages 227–229. IEEE, 1992.

[25] M. Artuso. Silicon sensors implemented on p-type substrates for high radiation resistance application. *Nucl. Instr. and Meth. A*, 582:835–838, 2007.

[26] U. Kötz et al. Silicon Strip Detectors with Capacitive Charge Division. *Nucl. Instr. and Meth. A*, 235:481–487, 1985.

[27] P. Luke. Single-polarity charge sensing in ionization detectors using coplanar electrodes. *Appl. Phys. Lett.*, 65:2884–2886, 1994.

[28] P. Luke, C.S. Tindall, and M. Amman. Proximity Charge Sensing With Semiconductor Detectors. *IEEE Trans. Nucl. Sci.*, 56:808–812, 2009.

[29] P. W. Cattaneo. Capacitances in micro-strip detectors: A conformal mapping approach. *Solid-State Electronics*, 54:252–258, 2010.

[30] E. Tuovinen. *Processing of Radiation Hard Particle Detectors on Czochralski Silicon*. PhD thesis, Helsinki University of Technology, 2008. ISBN 978-952-10-3727-6.

[31] J. Härkönen et al. Radiation hardness of Czochralski silicon, Float Zone silicon and oxygenated Float Zone silicon studied by low energy protons. *Nucl. Instr. and Meth. A*, 518:346–348, 2004.

[32] T. Kohriki et al. First observation of thermal runaway in the radiation damaged silicon detector. *IEEE Trans. Nucl. Sci.*, 43:1200–1202, 1996.

[33] G. Lindström et al. Radiation hard silicon detectors — developments by the RD48 (ROSE) collaboration. *Nucl. Instr. and Meth. A*, 466:308–326, 2001.

[34] C. Da Via et al. Advances in silicon detectors for particle tracking in extreme radiation environments. *Nucl. Instr. and Meth. A*, 509:86–91, 2003.

[35] V. Eremin, E. Verbitskaya, and Z. Li. Effect of radiation induced deep level traps on Si detector performance. *Nucl. Instr. and Meth. A*, 476:537–549, 2002.

[36] V. Eremin, J. Härkönen, Z. Li, and E. Verbitskaya. Current injected detectors at super-LHC program. *Nucl. Instr. and Meth. A*, 583:91–98, 2007.

[37] N. Doble, L. Gatignon, G. von Holtey, and F. Novoskoltsev. The upgraded muon beam at the SPS. *Nucl. Instr. and Meth. A*, 343:351–362, 1994.

[38] Particle Data Group. Review of Particle Physics. *J. Phys. G*, 33:1–1232, 2006.

[39] K. Klein. The CMS Silicon Strip Tracker – Overview and Status. *Proceeding of Science*, HEP(2005):378–378/4, 2005.

[40] W.C. Sailor et al. A model for the performance of silicon microstrip detectors. *Nucl. Instr. and Meth. A*, 303:285–297, 1991.

[41] E. Del Monte et al. Scientific performances of the XAA1.2 front-end chip for silicon microstrip detectors. *Nucl. Instr. and Meth. A*, 572:708–721, 2007.

[42] O. Toker, S. Masciocchi, E. Nygård, A. Ritdge, and P . Weilhammer. VIKING, a CMOS low noise monolithic 128 channel frontend for Si-strip detector readout. *Nucl. Instr. and Meth. A*, 340:572–579, 1994.

[43] I. Kipnis et al. A Time-over-Threshold Machine: the Readout Integrated Circuit for the BABAR Silicon Vertex Tracker. *IEEE Trans. Nucl. Sci.*, 44(3):289–297, 1997.

[44] L. Jones et al. The APV25 deep submicron readout chip for CMS detectors. In *5th Conference on Electronics for LHC Experiments, Snowmass, CO, USA*, pages 162–166, 1999.

[45] C. Bloch. Commissioning of the CMS Tracker Outer Barrel. In *9th* ICATPP *Conference on Astroparticle, Particle, Space Physics, Detectors and Medical Physics Applications*, pages 1038–1043, 2005. Como, Italy, 17 – 21 Oct 2005.

[46] J. Härkönen et al. The Cryogenic Transient Current Technique (C-TCT) measurement setup of CERN RD39 Collaboration. *Nucl. Instr. and Meth. A*, 581:347–350, 2007.

[47] L. Jones. APV25-S1 User Guide version 2.2. Technical report, RAL Microelectronics Design Group, Sept. 2001.

[48] F. Campabadal et al. Design and performance of the ABCD3TA ASIC for readout of silicon strip detectors in the ATLAS semiconductor tracker. *Nucl. Instr. and Meth. A*, 552:292–238, 2005.

[49] G. Aad et al. The ATLAS experiment at the CERN LHC. *J. Instrum.*, 3:S08003, 2008.

[50] T. Mäenpää. The Finnish CMS-TOB Cosmic Muon Telescope. Licentiate thesis, Helsinki University, 2006.

[51] C. Eklund and E. Pietarinen. ROxi: read-out cross interface for high speed data acquisition applications. HU-SEFT RD 1995 - 06.

[52] S.A. Baird et al. A PMC based ADC card for CMS Tracker readout. Technical report, CLRC Rutherford Appleton Laboratory.

[53] C. Foudas et al. The CMS tracker readout front end driver. *IEEE Trans. Nucl. Sci.*, 52(6):2836–2840, 2005.

[54] F. Drouhin et al. The CERN CMS Silicon Strip Tracker Control System. In *NSS MIC SNPS and RTSD Conference proceedings*, Roma, Italy, Oct 2004.

[55] F. Drouhin et al. The control system for the CMS Tracker front-end. In *IEEE Nuclear Science Symposium Conference Record*, volume 2, pages 10–6–10–10, 2000.

[56] G.Magazzu et al. The Detector Control Unit: An ASIC for the Monitoring of the CMS Silicon Tracker. *IEEE Trans. Nucl. Sci.*, 51(4):1333–1336, 2004.

[57] R. Bainbridge et al. Commissioning Procedures and Software for the CMS Silicon Strip Tracker. In *Proceedings of the Computing in High Energy and Nuclear Physics conference*, Feb. 2006.

[58] M. D'Alfonso et al. Validation tests of the CMS TIB/TID structures. *CMS NOTE*, 2009/010.

[59] N. Amos et al. Position resolution of msgcs with cathode readout. *Nucl. Instr. and Meth. A*, 384:342–250, 1997.

[60] L. Silvestris. Silicon Tracking in CMS. *Nuclear Physics B (Proc. Suppl.)*, pages 239–248, 2003.

[61] V. Karimäki. Explicit Covariance Matrix for Particle Measurement Precision. HIP-1997-48/EXP, 1997.

[62] T. Lampén et al. Alignment of the Cosmic Rack with the Hits and Impact Points Algorithm. *CMS NOTE*, 2006/006.

[63] P. Schleper, G. Steinbrück, and M. Stoye. Software Alignment of the CMS Tracker using MILLEPEDEII. *CMS NOTE*, 2006/011.

[64] Hans Bichsel. A method to improve tracking and particle identification in tpcs and silicon detectors. *Nucl. Instr. and Meth. A*, 562(1):154–197, 2006.

[65] K. S. Kölbig and B. Schorr. A program package for the Landau distribution. *Comp. Phys. Comm.*, 31:97–111, 1984.

[66] CMS Collaboration. Commissioning and Performance of the CMS Silicon Strip Tracker with Cosmic Ray Muons. *J. Instrum.*, 5:T03008, 2010.

[67] M. Brigida, C. Favuzzi, P. Fusco, F. Gargano, N. Giglietto, F. Giordano, F. Loparco, B. Marangelli, M.N. Mazziotta, N. Mirizzi, S. Rain, and P. Spinelli. A new Monte Carlo code for full simulation of silicon strip detectors. *Nucl. Instr. and Meth. A*, 533(3):322–343, 2004.

[68] M. Krammer. Position resolution and charge collection efficiency. *Nucl. Instr. and Meth. A*, 386:193–200, 1997.

[69] J. Straver et al. One micron spatial resolution with silicon strip detectors. *Nucl. Instr. and Meth. A*, 348:485–490, 1994.

[70] M. Demarteau et al. Characteristics of the Outer Layer Silicon Sensors for the Run IIb Silicon Detector. *DØ note 4308*, 2003.

[71] M. Köhler et al. Test Beam Measurements with 3D Silicon Strip Detectors. In *Proceedings of the 11th ICATPP Conference on Astroparticle, Particle, Space Physics, Detectors and Medical Physics Applications*, Villa Olmo, Como, Oct. 2009.

[72] D. Pitzl et al. Type inversion in silicon detectors. *Nucl. Instr. and Meth. A*, 311:98–104, 1992.

[73] A. Longoni, M. Sampietro, and L. Strüder. Instability of the Behaviour of High Resistivity Silicon Detectors due to the Presence of Oxide Charges. *Nucl. Instr. and Meth. A*, 288:35–43, 1990.

[74] M. Aguilar-Benítez et al. Construction and test of the final CMS Barrel Drift Tube Muon Chamber prototype. *Nucl. Instr. and Meth. A*, 480:658–669, 2002.

[75] M. Köhler et al. Beam Test Measurements With 3D-DDTC Silicon Strip Detectors on n-Type Substrate. *IEEE Trans. Nucl. Sci.*, 56(5):2987–2994, 2010.

List of Acronyms

AC	*Alternating current*	
ADC	*Analog to Digital Converter*	Here: Unit of analog data after acquisition
ALICE	*A Large Ion Collider Experiment*	One of the large LHC experiments
APV	*Analog Pipeline Version*	A read-out chip designed for the CMS tracker.
APV25		APV chip fabricated in the 0.25 μm process.
CCU	*Communication & Control Unit*	Name of an integrated circuit used at CMS Tracker
CERN		the European Organization for Nuclear Physics
CCE	*Charge Collecting Efficiency*	
CMN	*Common Mode Noise*	
CMS	*Compact Muon Solenoid*	One of the large LHC experiments
CoG	*Center of Gravity*	
CRack	*Cosmic Rack*	Name of an apparatus at CERN
DCU	*Detector Control Unit*	Name of an integrated circuit used at CMS Tracker
DUT	*Device Under Test*	
EMA	*Exponentially Moving Average*	
ENC	*Equivalent Noise Charge*	
FinnCRack	*Finnish Cosmic Rack*	A measurement apparatus
FED	*Front End Driver*	Name of a data-acquisition card
FWHM	*Full Width at Half Maximum*	
FZ	*Float Zone*	A method used to grow silicon crystals
HEP	*High Energy Physics*	
HIP	*Helsinki Institute of Physics*	
HIP	*Hit and Impact Point algorithm*	
HPK	*Hamamatsu Photonics K.K.*	Corporation producing, e.g., silicon detectors.
I^2C	*Inter-Integrated Circuit*	A Communication bus standard.
IOV	*Interval Of Validity*	
LG	*Landau and Gaussian function*	Convolution of these two functions
LHC	*Large Hadron Collider*	
MCz	*Magnetic Czochralski*	A method used to grow silicon crystals
MIP	*Minimum Ionizing Particle*	
MPV	*Most Probable Value*	
PC	*Personal Computer*	
PCB	*Printed Circuit Board*	
PMC	*Pci Mezzanine Card*	Daughter board interface, an IEEE standard.
ROxi	*Read-out Cross Interface*	Name of a data acquisition card
SAH	*Sample And Hold*	
SCSI	*Space Charge Sign Inversion*	
SiBT07	*Silicon Beam Telescope*	A measurement apparatus
SiBT99	*Silicon Beam Telescope*	Another measurement apparatus
SLHC	*Super-LHC*	
SNR	*Signal to Noise Ratio*	
SPS	*Super Proton Synchrotron*	One of the particle accelerators at CERN.
TIC	*Track-Induced Clustering*	
TOB	*Tracker Outer Barrel*	Part of CMS Tracker
VA1	*Viking Architecture 1*	The name of a readout chip by Ideas ASA.
VME	*VERSA Module Europe*	A computer bus standard
VUTRI	*Very Ultimate Tracker Readout Interface*	Name of a PCB used in the SiBT